Sparse genetic tracing reveals regionally specific functional organization of mammalian nociceptors

William Olson[1], Ishmail Abdus-Saboor[1†], Lian Cui[1†], Justin Burdge[1], Tobias Raabe[2], Minghong Ma[1], and Wenqin Luo[1*]

[1]Department of Neuroscience, Perelman School of Medicine, University of Pennsylvania, Philadelphia, PA 19104, USA

[2]Department of Genetics, Perelman School of Medicine, University of Pennsylvania, Philadelphia, PA 19104, USA

† These authors contributed equally to this work

* **Corresponding author:** Wenqin Luo, MD, PhD, Department of Neuroscience, Perelman School of Medicine, University of Pennsylvania, 145 Johnson Pavilion, 3610 Hamilton Walk, Philadelphia, PA 19104, USA. Email: luow@mail.med.upenn.edu

Abstract

The human distal limbs have a high spatial acuity for noxious stimuli but a low density of pain-sensing neurites. To elucidate mechanisms underlying the 'pain fovea', we sparsely traced non-peptidergic nociceptors across the body using a newly generated *MrgprD*^{CreERT2} mouse line. We found that mouse plantar paw skin also has a low density of MrgprD^{+} neurites, and individual arbors in different locations are comparable in size. Surprisingly, the central arbors of plantar paw and trunk innervating nociceptors have distinct morphologies in the spinal cord. This regional difference is well correlated with a heightened signal transmission for plantar paw circuits, as revealed by both spinal cord slice recordings and behavior assays. Taken together, our results elucidate a novel somatotopic functional organization of the mammalian pain system and suggest that regional central arbor structure could facilitate the magnification of plantar paw regions to contribute to the 'pain fovea'.

Introduction

The skin mediates physical contact with environmental mechanical, thermal, and chemical stimuli. As an animal moves through the world, certain parts of the skin are likely sites of "first contact" with these stimuli (for instance, the distal limbs, face/whiskers, and tail for quadrupedal mammals like mice). Therefore, these somatosensory regions require heightened sensitivity to fulfil behaviorally relevant functions, such as environment exploration.

Touch and pain are the two most important types of somatosensation for this functional purpose: touch allows for feature detection while pain prevents tissue damage. Indeed, classic work has defined important regional specialization of the nervous system for tactile sensation in these areas. Two mechanisms in the peripheral organization of the discriminative touch system facilitate high spatial acuity sensation in the primate distal limbs and mouse whisker pad. These are the *high innervation density* and *smaller receptive field sizes* of the primary light touch neurons, the Aβ mechanoreceptors, in these regions[1-7]. In contrast, the question of whether regional specialization exists in the mammalian pain system has remained elusive until recently. Upon stimulation using nociceptive-specific laser beams, human subjects show a heightened spatial acuity in the distal limbs (especially the fingertips) for pain stimuli, much like they do for touch stimuli[8-10]. This suggests that this region is also a "pain fovea". However, human fingertip skin has a relatively *low density of*

66 *pain-sensing neurites*[9]. While this suggests that region-specific organization likely
67 exists in pain circuits downstream of the periphery (i.e. central nervous system),
68 currently the exact neural mechanisms of the pain fovea are unclear.
69
70 Pain stimuli are detected by primary sensory neurons called nociceptors, which have
71 cell bodies in the dorsal root ganglia (DRG) or trigeminal ganglia (TG) and axons that
72 bifurcate into peripheral and central branches. The peripheral projection of a
73 nociceptor usually terminates as a free nerve arbor in the skin or deeper tissues, while
74 the central projection terminates in an arbor in the dorsal horn (DH) of the spinal cord
75 or caudal medulla. Though previous work has mapped the peripheral receptive fields
76 or traced the central terminals of mammalian nociceptors[11-21], these studies have not
77 established a model for the somatotopic functional organization of the mammalian
78 pain system due to the limited number of neurons traced from restricted skin regions.
79
80 We therefore sought to reveal the region-specific organization of mammalian
81 nociceptors across the entire somatotopic map. We generated a novel *MrgprD*^{CreERT2}
82 mouse line to perform systematic sparse genetic tracing of a population of
83 non-peptidergic nociceptors that mediate mechanical pain and beta-alanine (B-AL)
84 triggered itch[22, 23]. We chose these nociceptors because they are the most abundant
85 type of cutaneous nociceptor and they likely correspond to the main type of free nerve
86 terminals stained with anti-PGP9.5 antibody in previous human skin biopsy data[9, 24].

Indeed, like the human skin biopsy results, we found that MrgprD^{+} neurites have a comparatively low neurite density in plantar paw compared to trunk skin. In addition, and in contrast to the Aß mechanoreceptors, sparse genetic tracing revealed that the arbor field sizes of individual nociceptors are comparable between different skin regions, whereas plantar paw and trunk innervating nociceptors display distinct morphologies in their central terminals. Lastly, using *MrgprD*^{CreERT2}; *Rosa*$^{ChR2\text{-}EYFP}$ mice, we specifically activated these nociceptors using blue laser light during *in vitro* spinal cord slice recordings and during behavior assays. We found that, while almost all layer II DH neurons in all locations receive direct MrgprD^{+} afferent input, the optical threshold required to induce postsynaptic responses is much lower in plantar paw regions. This was paralleled by a decrease in the light intensity threshold required to elicit a withdrawal response in paw, compared to upper thigh, skin stimulation. Collectively, we have identified a previously unappreciated somatotopic difference in the functional organization of mammalian nociceptors. Our anatomical, physiological, and behavior data suggest that region-specific central arbor structure could help to magnify the representation of plantar paw nociceptors in the DH to establish the 'pain fovea'.

Results

Generation and specificity of *MrgprD*^{CreERT2} mice

Given that previous descriptions of nociceptor structure have not allowed for

systematic comparisons between body regions, we sought to use sparse genetic labeling to trace single nociceptor morphologies across the entire somatotopic map. We generated a mouse line in which a tamoxifen-inducible Cre (CreERT2) cassette is knocked into the coding region of Mas-related gene product receptor D (*MrgprD*) (Figure 1A, Figure S1). Consistent with the previous finding that *MrgprD* is expressed more broadly in early development than in adulthood[25], early embryonic (E16.5-E17.5) tamoxifen treatment of $MrgprD^{CreERT2}$ mice labels MrgprD$^+$ neurons along with non-peptidergic neurons expressing other *Mrgpr* genes, such as *MrgprA3* and *MrgprB4* (Figure S2). In contrast, when we crossed $MrgprD^{CreERT2}$ mice with a Cre-dependent $Rosa^{ChR2\text{-}EYFP}$ line and provided postnatal (P10-P17) tamoxifen treatment (Figure 1B), MrgprD$^+$ non-peptidergic nociceptors were specifically labeled. We examined these treated mice at 4 postnatal weeks or older (>4pw), a time point at which MrgprD$^+$ non-peptidergic nociceptors have completely segregated from other Mrgpr$^+$ DRG neurons[25]. We found that ChR2-EYFP$^+$ DRG neurons bind IB4 (a marker for non-peptidergic DRG neurons) but do not express CGRP (a marker for peptidergic DRG neurons)[24] (Figure 1C), and ChR2-EYFP$^+$ DH terminals similarly overlap with IB4 but not CGRP (Figure 1G). Double *in situ* hybridization demonstrated that this strategy efficiently labels DRG neurons expressing *MrgprD* (88.1 ± 1% of ChR2-EYFP$^+$ neurons, n = 3 animals) but not those expressing *MrgprA3* (1.4 ± 0.1%) or *MrgprB4* (0.4 ± 0.3%) (Figure 1D-F). Almost all *MrgprD* expressing neurons were labeled with ChR2-EYFP (92.9 ± 4.6% of $MrgprD^+$

neurons) by this treatment. Therefore, this newly generated inducible *MrgprD*^{CreERT2} line allows for the specific and efficient targeting of adult MrgprD^{+} nociceptors.

We then sought to trace individual MrgprD+ non-peptidergic nociceptors using sparse genetic labeling. When crossed with a Cre-dependent alkaline phosphatase reporter line (*Rosa*^{iAP}), we found that sparse recombination occurs in the absence of tamoxifen treatment (Figure 2A&B). This background recombination labels 3-11 neurons/DRG (5.2 ± 1.6 neurons/DRG, *n* = 47 DRGs from 3 animals) in 3-4 pw animals (Figure 2C), which represents <1% of the total MrgprD^{+} nociceptor population[24, 26, 27]. The sparsely labeled DRG neurons co-express non-peptidergic nociceptor markers peripherin, PAP[28], and RET (Figure 2D, F, H), but do not express NF200 or CGRP (Figure 2E, G). To further determine the specificity of this sparse recombination, we used an *MrgprD*^{EGFPf} knock-in line[24], in which expression of EGFP mimics the dynamic expression of endogenous *MrgprD*. We generated *MrgprD*$^{CreERT2/EGFPf}$; *Rosa*^{iAP} mice and found that almost all AP^{+} neurons co-express *MrgprD*^{EGFPf} (93. 7 ± 2.3%, *n* = 126 AP^{+} neurons from 3 animals) (Figure 2I) in 3 to 4pw mice. This result indicates that, although *MrgprD* is broadly expressed during early development, this background recombination occurred preferentially in adult MrgprD^{+} nociceptors.

Genetic tracing of MrgprD^{+} skin terminals reveals a relatively comparable organization in the periphery

MrgprD$^+$ neurons innervate both hairy and glabrous skin and are the most abundant class of cutaneous free nerve arbors[24]. To systematically compare the peripheral single-cell structure of mammalian pain neurons across the somatotopic map, we performed whole mount colorimetric AP staining using untreated 3-4 pw *MrgprD*^{CreERT2}; *Rosa*^{iAP} skin.

We found that 98.4% (130/132 arbors, n = 4 animals) of single-cell arbors have a "bushy ending" morphology (Figure 3A&B, D&E, Figure S3A)[29], featuring thickened terminal structures in the epidermis. The distal ends of arbors in glabrous plantar paw skin have single, un-branched thickened neurites (Figure 3A&B), while arbors in the hairy skin feature both un-branched neurites as well as dense neurite clusters (Figure 3D&E). These dense clusters are seen in all analyzed regions that have hairy skin and likely innervate the necks of hair follicles (red arrowheads in Figure 3E&F) (see also Figure S5C)[24]. A very small minority (1.6%) of arbors in the hairy skin have "free endings"[29] lacking these thickened structures (Figure S3A-C).

MrgprD$^+$ non-peptidergic nociceptive field sizes range from 0.08 to 0.9 mm^2, with the smallest average field size found in the head skin between the ears and in the proximal limbs (Table 1, Figure 3G). Interestingly, non-peptidergic nociceptors innervating the distal limbs (plantar and dorsal paw skin) have average arbor sizes close the middle of this range, and distal limb and trunk arbors are comparable in size

(Table 1, Figure 3G&H). In addition, consistent with human skin[8], whole-population labeling of MrgprD$^+$ fibers using tamoxifen (0.5 mg at P11) reveals that the overall neurite density is slightly lower in the paw glabrous skin compared to trunk hairy skin (Figure 3C&F). In short, in contrast to mammalian Aβ mechanoreceptors, plantar paw innervating mouse non-peptidergic nociceptors do not display higher neurite density or smaller receptive field sizes.

MrgprD$^+$ nociceptors show regionally distinct organization in their central arbors

Since the peripheral organization of MrgprD$^+$ non-peptidergic nociceptors does not exhibit an obvious mechanism to facilitate heightened sensitivity in the plantar paw, we next used whole mount AP staining of untreated 3-4 pw *MrgprD*^{CreERT2}; *Rosa*^{iAP} spinal cords to compare their central arbors between regions. Non-peptidergic nociceptor central branches enter the spinal cord through the dorsal root, travel rostrally or caudally for 0 to 3 segments, and then dive ventrally to establish arbors in layer II of the DH (Table 2)[24]. Most MrgprD$^+$ central branches do not bifurcate (65.8%, n = 234 neurons from 3 animals), and most also terminate within the segment of entry (72.6%) (Table 2). However, some (34.2%) bifurcate one or more times in the spinal cord, and some (27.3%) travel up to 3 segments from the point of entry (Table 2). For the central branches that bifurcate, most of their secondary/tertiary branches join other branches from the same neuron to co-form one axonal arbor,

while some end with a second arbor or terminate in the spinal cord without growing an arbor (Table 2, Figure S4A&B). The majority (91.9%) of labeled nociceptors have only one arbor, but a few have no (0.4%), 2 (6.8%), or 3 (0.9%) central arbors (Table 2).

Strikingly, MrgprD^{+} non-peptidergic nociceptor central arbors display two different morphologies that can be distinguished by the ratio of their mediolateral width to their rostrocaudal height (W/H ratio) (Figure 4H). We defined arbors with W/H ratios >0.2 as "round" (Figure 4A-C, H, and Table 3) and arbors with W/H ratios <0.2 as "long and thin" (Figure 4B-F, H, and Table 3). Further, these morphological types are regionally segregated. Round arbors are found in DH regions known to represent the distal limbs (medial cervical and lumbar enlargements) as well as tail, anogenital (sacral DH), and head/face (descending trigeminal terminals in the upper cervical DH and medulla) skin (Figure 4B&C, H, J, and Figure S4C)[30, 31]. Long arbors are instead located in regions corresponding to the proximal limbs (lateral cervical and lumbar enlargements) and trunk skin (thoracic DH) (Figure 4B-F, H, J)[30-32]. While round and long arbors differ in morphology, they do not differ in area (Figure 4G).

In the cervical and lumbar enlargements (C3-C6, L3-L6), the medial DH contains a curved zone of round arbors that is encircled by laterally located long arbors (Figure 4C). Somatotopic mapping of the cat and rat DH indicates that this medial curved

zone in the lumbar enlargement matches the representation of the plantar paw and digits, with the dorsal paw and proximal limb representations lying more laterally[30, 31, 33-38]. We compared the number of labeled peripheral arbors in the toe and plantar paw skin with the number of round DH terminals in the corresponding half of the lumbar enlargement. This showed a very close correlation (Figure 4I), supporting that the round central arbors of the lumbar enlargement correspond to plantar paw and digit MrgprD$^+$ nociceptors, while nociceptors from other regions of the hindlimb (including dorsal hindpaw and proximal hindlimb) grow long central arbors located more laterally.

Since <1% of MrgprD$^+$ neurons are traced in these mice, it remains possible that this round-vs.-long arbor regional distinction may be an artifact of sparse labeling. For example, if both types were found throughout the DH but were differentially enriched between regions, sparse labeling might only trace the most prevalent type in each location. Using increasing dosages of tamoxifen, we found that these arbor types occupy mutually exclusive zones of the DH (Figure 5A-F). The maintained segregation of long and round arbors in the DH despite the increased number of AP$^+$ DRG neurons indicates that these arbor morphologies represent a true somatotopic distinction among MrgprD$^+$ non-peptidergic nociceptors.

Neighboring non-peptidergic nociceptors highly overlap in the skin and spinal

cord

The axonal arbors of some somatosensory neurons have a non-overlapping arrangement between neighbors ("tiling") in the body wall of the fly and zebrafish[39, 40]. To determine if mammalian non-peptidergic nociceptive arbors tile in the skin, we generated double knock-in *MrgprD*$^{CreERT2/EGFPf}$; *Rosa*^{tdTomato} mice. After low-dose tamoxifen treatment, sparsely labeled MrgprD^{+} neurons in these mice express tdT while the entire population expresses EGFPf. The arbor fields of individual double tdT^{+}/EGFP^{+} neurons are always co-innervated by EGFP^{-}only^{+} fibers in both hairy and glabrous skin (Figure S5A-D), indicating that peripheral arbors of neighboring non-peptidergic nociceptors do not tile but instead overlap extensively. In hairy skin, sparse labeled tdT^{+} neurites co-innervated hair follicles with EGFP-only^{+} fibers, indicating that multiple MrgprD^{+} neurons can innervate single hair follicles. Similarly, both round and long DH arbors of non-peptidergic nociceptors highly overlap with their neighbors in the DH (Figure S5E&F).

Heightened signal transmission in the paw DH circuitry of MrgprD+ neurons

Next, given the striking somatotopic differences in the central arbor organization of MrgprD^{+} nociceptors, we asked whether we could find regional (plantar paw vs. trunk) differences in the transmission of sensory information at the level of the dorsal horn. We generated *MrgprD*^{CreERT2}; *Rosa*$^{ChR2\text{-}EYFP}$ mice, which were treated with

255 postnatal tamoxifen (>P10, Figure 1), to compare the synaptic transmission of these
256 neurons between somatotopic regions in spinal cord slice recordings. Comparable
257 expression of ChR2-EYFP, as measured by the native fluorescence intensity, was
258 found for MrgprD^{+} neurons in thoracic (T9-T12) and hind limb-level (L3-L5) DRGs
259 (Figure S6). We first used *MrgprD*^{CreERT2}; *Rosa*$^{ChR2\text{-}EYFP/ChR2\text{-}EYFP}$ mice (carrying two
260 copies of the *Rosa*$^{ChR2\text{-}EYFP}$ allele) to perform *in vitro* whole-cell patch-clamp
261 recordings of layer II interneurons located in the territory innervated by ChR2-EYFP^{+}
262 fibers in transverse spinal cord sections (Fig. 6A). Light-evoked excitatory
263 postsynaptic currents ($EPSC_L$s) in these neurons could be differentiated into
264 monosynaptic or polysynaptic responses based on latency, jitter, and response failure
265 rate during 0.2 Hz blue light stimulation (Figure 6B&C)[41]. Almost all recorded
266 neurons in both medial and lateral lumbar DH showed $EPSC_L$s (Figure 6D, Table 4),
267 with most cells (14/17 = 82.4% in medial lumbar, 14/16 = 86.5% in lateral lumbar)
268 showing monosynaptic $EPSC_L$s in both locations. This indicates that the majority of
269 DH neurons in this innervation territory receive direct MrgprD^{+} input, and that the
270 incidence receiving direct input is equivalent for medial lumbar and lateral lumbar
271 DH.
272
273 Given the very high level of ChR2 expression in these mice, any potential difference
274 between the medial and lateral lumbar spinal cord may be masked by a “ceiling”
275 effect. We therefore halved the genetic dosage of *Rosa*$^{ChR2\text{-}EYFP}$ by taking slices from

276 *MrgprD*$^{CreERT2;}$ *Rosa*$^{ChR2\text{-}EYFP/+}$ mice. Interestingly, we saw a dramatic difference when
277 comparing the medial and lateral lumbar DH of double heterozygous mice. Medial
278 lumbar DH neurons showed a much higher incidence of light responses than lateral
279 lumbar neurons, with a ~9-fold more (15/17 = 88.2% vs. 2/19 = 10.5%) in the
280 incidence of monosynaptic $EPSC_L$s over lateral lumbar neurons (Figure 6E, Table 4).
281 Similar to the lateral lumbar DH, the incidence of monosynaptic $EPSC_L$s of layer II
282 neurons in the medial and lateral thoracic region are also very low (1/11 = 9.1%)
283 (Figure 6E, Table 4) . Moreover, even among responsive neurons, the pulse duration
284 threshold required to elicit $EPSC_L$s was much longer in lateral lumbar and thoracic
285 DH neurons compared to medial lumbar neurons (Figure 6F). These results showed a
286 lower threshold for light-trigged excitatory currents in medial lumbar compared to
287 lateral lumbar and thoracic DH neurons, suggesting a heightened signal transmission
288 in plantar paw circuits. We repeated these recordings in sagittal spinal cord slices and
289 similarly found a higher $EPSC_L$ incidence in medial lumbar compared to lateral
290 lumbar or thoracic DH (Table 4). This confirms that these differences are not caused
291 by the different orientation of nociceptors in round vs. long arbor regions. Taken
292 together, our results show that, while most DH neurons in the MrgprD$^+$ innervation
293 territory receive direct MrgprD$^+$ input, the overall signal transmission is heightened in
294 plantar paw compared to trunk nociceptive circuits. This heightened transmission was
295 seen specifically at the level of nociceptor-to-DH neuron connections, and it
296 correlates closely with the region-specific organization of MrgprD$^+$ central arbors.

297

298 **Plantar paw MrgprD^{+} nociceptors have a lower stimulation threshold to induce**

299 **avoidance behaviors**

300 Finally, since we saw a regional increase in signal transmission in plantar paw DH

301 MrgprD^{+} circuits, we asked whether this has functional relevance for a freely

302 behaving animal. To activate ChR2 in skin-innervating nociceptors of behaving mice,

303 we stimulated *MrgprD*^{CreERT2}; *Rosa*$^{ChR2\text{-}EYFP/ChR2\text{-}EYFP}$ (*MrgprD-ChR2*) and

304 *Rosa*$^{ChR2\text{-}EYFP/ChR2\text{-}EYFP}$ (*Control*) mice (P10-17 tamoxifen treatment) at both the paw

305 and upper-thigh leg skin (Figure 7B&E) with either 473nm blue light or 532nm green

306 light as a negative control. High levels of ChR2-EYFP were expressed in peripheral

307 neurites in both plantar paw and upper leg skin (Figure 7A&D). Consistent with the

308 AP labeling (Figure 3), upper leg skin shows a much higher density of EYFP+

309 neurites than the paw glabrous skin (Figure S6A-C).

310

311 We first stimulated the paw skin of both groups of mice with green light (5mW, 10

312 Hz, sine wave) and observed no avoidance behavior such as paw withdrawal (Figure

313 7C, Videos 1&2). When we stimulated both groups of mice with 1mW of blue light

314 (10 Hz, sine wave), control mice did not respond, while 12.5% of *MrgprD-ChR2* mice

315 displayed light-induced paw withdrawal (Figure 7B&C). When stimulated with 5mW

316 blue light (10 Hz, sine wave), 100% of *MrgprD-ChR2* mice displayed clear

317 light-induced avoidance behavior responses consisting of paw withdrawal, high

318 frequency paw shakes, occasional licking, extended holding of the paw in the air, and
319 paw guarding. Control mice still did not respond (Figure 7B&C, Figure S7E, Videos
320 3&4).
321
322 Strikingly, when we activated MrgprD^{+} neurites in the shaved upper-thigh skin,
323 neither control nor *MrgprD-ChR2* mice responded to 5mW blue light (Figure 7E&F,
324 S6E, Videos 5&6). Rather, to observe a fully penetrant avoidance behavior response
325 in the upper-thigh of *MrgprD-ChR2* mice, the blue light power intensity had to be
326 increased to 10 or 20 mW (2-4 times higher than the requirement in the paw) (Figure
327 7E-G, Videos 7&8). When taking the temporal delay of avoidance responses (Figure
328 7H) into consideration, 20mW intensity blue light is required at the leg to trigger
329 responses comparable to 5mW intensity stimulation of the paw. In short, the light
330 intensity threshold required to trigger an avoidance response is significantly lower in
331 the paw compared to the upper-limb of *MrgprD-ChR2* mice.
332
333 Taken together, we have demonstrated a novel region-specific functional organization
334 in the dorsal spinal cord for the mammalian pain system, which is consistent across
335 anatomical, physiological, and behavioral levels.
336
337 **Discussion**
338 In this study, we identified a novel somatotopic organization in the central arbors of

mammalian MrgprD$^+$ nociceptors, which is very well correlated with a regional increase in the sensitivity of paw nociceptive circuits to external stimuli. Our results suggest a model in which region-specific central arbor structure contributes to a sensory "fovea" for pain (Fig. 7I). In this model, the wider mediolateral spread of plantar paw nociceptor central arbors could facilitate "afferent magnification"[42] in downstream CNS circuits and facilitate heightened pain sensitivity of the plantar paw. Remarkably, two features of mouse non-peptidergic nociceptors revealed by our study, the peripheral neurite density distribution and the nociceptive fovea location (the distal limb), are consistent with findings in humans[8-10]. Therefore, the organizational mechanisms we discovered in mice are likely to be conserved in human, which provides a possible explanation for the human "pain fovea".

MrgprD^{CreERT2} allows for specific targeting of adult MrgprD$^+$ nociceptors

Adult mice have two functionally distinct DRG neuronal populations expressing Mas-related gene product receptor (*Mrgpr*) genes. One expresses *MrgprA, MrgprB,* and *MrgprC* genes and the other only expresses *MrgprD*[23, 25, 43-47]. MrgprA/B/C$^+$ neurons also transiently express *MrgprD* during early development [25]. To specifically target MrgprD$^+$ neurons, we generated a new inducible *MrgprD^{CreERT2}* mouse line that allows for temporally controlled recombination. We demonstrated that postnatal (P10 or later) tamoxifen treatment of *MrgprD^{CreERT2}* mice specifically targets MrgprD$^+$ but not MrgprA/B/C$^+$ neurons (Figure 1).

To our advantage, we also found that sparse recombination in untreated *MrgprD*^{CreERT2}; *Rosa*^{iAP} mice is very specific for MrgprD$^+$ neurons (~94% AP$^+$ neurons are MrgprD$^+$, Figure 2I). We noticed that most of this random recombination likely occurs postnatally, as untreated *MrgprD*^{CreERT2}; *Rosa*^{iAP} tissue at P7 or younger shows no AP$^+$ neurons (data not shown). This temporal delay of recombination, along with the fact that there are many more adult MrgprD$^+$ than MrgprA/B/C$^+$ neurons [25, 43, 45, 46], likely contributes to the specificity of sparse AP labeling in these mice.

In this paper, we used prenatal tamoxifen treatment of *MrgprD*^{CreERT2} mice for two experiments: *MrgprD*$^{CreERT2/EGFPf}$; *Rosa*^{tdTomato} labeling to show nociceptor overlap (Figure S5) and increasing density labeling (Figure 5). In these experiments, both MrgprD$^+$ and MrgprA/B/C$^+$ neurons could be targeted. For the overlap experiment, neurites were chosen that had both red (*MrgprD*^{CreERT2} ; *Rosa*^{tdTomato}) and green (*MrgprD*^{EGFPf}) fluorescence, indicating these were MrgprD$^+$ neurites. For the increased density labeling experiment, even with high dosage (population-level) prenatal tamoxifen treatment of this line, MrgprA/B/C$^+$ neurons make up <20% of the total cells labeled (Figure S2). Given the nature of this experiment, we believe that our interpretation is not confounded by this issue.

Peripheral features of MrgprD$^+$ nociceptors show no obvious mechanism for the

sensory "fovea"

Though previous studies have traced various cutaneous somatosensory neurons, no systematic characterization of nociceptor morphology across the somatotopic map has been performed. In the periphery, sparse tracing of *Pou4f1* expressing somatosensory neurons (which includes almost all somatosensory DRG neuron classes[48]) in the back hairy revealed a "bushy ending" morphological type[29]. The authors suggested these terminals might correspond to C-fiber nociceptors or thermoceptors. In addition, MrgprB4$^+$ and TH$^+$ C fibers , which mainly mediate light touch but not pain, and innervate hairy skin only, have been genetically traced and analyzed[46, 49]. MrgprB4$^+$ neurons innervate the skin in large patches of free terminals[46], while TH$^+$ neurons form lanceolate endings around hair follicles[49]. To our knowledge, single-cell tracing has not previously been performed for any C-fiber nociceptors innervating the glabrous skin.

MrgprD$^+$ nociceptors innervate both hairy and glabrous skin but not deep tissues[24], making this population ideal for analysis of somatotopic differences. Our *MrgprD*^{CreERT2} tracing reveals that MrgprD$^+$ nociceptors display a bushy-ending morphology in hairy skin and thickened endings in the epidermis in the glabrous skin (the plantar paw and finger tips) (Figure 3, Figure S3). Very rarely, we found "free ending" terminals that lack thickened epidermal ending (Figure S3). These match the morphology and size of MrgprB4$^+$ light touch neurons[46], possibly indicating very rare

402 labeling of this subset. The fact that <2% of hairy skin terminals displayed this
403 morphology further supports the specificity of *MrgprD*^{CreERT2} sparse recombination.
404
405 Using genetic tracing, we found that (1) the density of MrgprD^{+} C fiber nociceptive
406 neurites is slightly lower in paw (including digit tips) compared to trunk skin and (2)
407 paw and trunk terminals are comparable in the overall area (Figure 3). This second
408 result contrasts with an earlier study that performed single-fiber recordings of human
409 mechanically responsive C-fiber units, which saw smaller receptive fields in the distal
410 leg[11]. This discrepancy could be caused by differences between species, techniques
411 (physiological vs. direct anatomic tracing), or the composition of neurons that were
412 analyzed (the previous study presumably recorded from multiple molecular classes).
413 In short, in our analysis of MrgprD^{+} nociceptors, we did not find any obvious
414 peripheral mechanism that might readily explain the heightened pain acuity of the
415 distal limbs seen in human subjects or the increased sensitivity of the mouse plantar
416 paw to *in vivo* optogenetic skin stimulation (Figure 7).
417
418 **MrgprD^{+} nociceptors display region specific organization of central circuits**
419 Classic studies have characterized the single-cell central arbors of C-fiber afferents
420 using Golgi staining or backfill techniques and described them as
421 longitudinally-oriented “thin sheets” that are short in the mediolateral axis and
422 extended in the rostrocadual axis[18, 19, 50]. This description corresponds well to the

423 "long arbors" we found in DH zones representing proximal limb and trunk regions
424 (Figure 4). The central terminals of MrgprB4^{+} and TH^{+} C-fiber light touch neurons
425 also match this long terminal morphology, consistent with the fact that these classes
426 only innervate hairy skin[46, 49]. Nevertheless, a systematic comparison of nociceptive
427 central terminals across the entire somatotopic map has not been conducted.
428
429 Here, we found regionally distinctive central arbor organization among MrgprD^{+}
430 nociceptors; those innervating the distal limbs, tail, anogenital skin, and the head/face
431 display round central terminals, while those innervating the trunk hairy skin display
432 long and thin central arbors (Figure 4). Given that neurons in the medulla and sacral
433 spinal cord display round arbors (Figure 4 and S4C), this morphological difference
434 does not correlate with hairy vs. glabrous skin regions but instead seems to correlate
435 with regions located at the extremities. In addition, we found that regions with round
436 arbors showed an increased signal transmission onto downstream neurons, and a
437 heighted sensitivity to external stimulation (Figures 6, 7, and S7). These results
438 suggest that region specific central arbors of MrgprD+ nociceptors are an important
439 component for the region-specific spinal cord circuits. Taken together, we have
440 uncovered a novel form of region-specific functional organization for mammalian
441 nociceptors.
442

Some previous studies suggest that the third-order DH collaterals of Aβ mechanoreceptors are also wider (in the mediolateral axis) in the medial lumbar enlargement compared to other DH regions[34, 51, 52]. However, the primary signal transmission for discriminative information occurs in the dorsal column nuclei but not the dorsal spinal cord. Thus, it is currently less clear whether this central arbor morphological difference contributes to differential touch sensitivity.

Region-specific DH circuit organization leads to an increased sensitivity of paw pain circuits to external input

Finally, we determined the stimulus threshold (laser power) required to trigger avoidance behaviors of freely behaving *MrgprD-ChR2* mice upon paw or upper leg skin light stimulation. While 100% of tested animals showed withdrawal responses when 5 mW blue light was applied to the plantar paw, a 4-fold increase in light intensity (20 mW) was required to trigger comparable responses (in terms of rate and latency) in the upper leg (Figure 7, Figure S6B). Thus, our experiments show a clear heightened sensitivity of plantar-paw-innervating MrgprD$^+$ nociceptors to stimulation. Interestingly, our use of peripheral optogenetic stimulation likely bypasses the effects of some peripheral parameters, such as the physical properties of the skin or the expression of molecular receptors, on the sensation of natural stimuli. Thus, this approach allowed us to more directly compare and probe the effects of circuit organization mechanisms on region-specific sensitivity.

Collectively, our results suggest that region-specific MrgprD$^+$ central arbor organization could magnify the representation of the plantar paw within pain circuits to contribute to a nociceptive "fovea" [52] (Figure 7I). This central organization mechanism could allow for the sensitive detection of harmful stimuli in these areas, despite a lower neurite density in the periphery. This finding is relevant for pain research using mouse models, which has historically relied heavily on pain assays in plantar paw/medial lumbar circuits[53]. Given our findings, it would be interesting to examine whether region-specific differences exist in the molecular and physiological pathways of acute and/or chronic pain models. Such work could be informative for the translation of preclinical models to clinical treatment.

Online Methods

Mouse strains:

Mice were raised in a barrier facility in Hill Pavilion, University of Pennsylvania. All procedures were conducted according to animal protocols approved by Institutional Animal Care and Use Committee (IACUC) of the University of Pennsylvania and National Institutes of Health guidelines. *Rosa*^{tdTomato}, *Rosa*^{iAP}, *Rosa*$^{ChR2\text{-}EYFP}$, and *MrgprD*^{EGFPf} lines have been described previously[24, 54-56].

Generation of *MrgprD*^{CreERT2} mice:

Targeting construct arms were subcloned from a C57BL/6J BAC clone (RP24-316N16) using BAC recombineering, and the CreERT2 coding sequence followed by a FRT-flanked neomycin-resistance selection cassette was engineered in-frame following the *MrgprD* starting codon by the same approach (Figure S1A). The targeting construct was electroporated into a C57/129 hybrid (V6.5) mouse embryonic stem cell line by the Penn Gene Targeting Core. ES clones were screened by PCR using primers flanking the 3' insertion site (Figure S1C). Positive clones were further screened using Southern blot with both internal and external probes (Figure S1B). The Penn Transgenic Core assisted in *MrgprD*^{CreERT2} ES clone blastocyst injection and in the generation of chimeric mice, which were mated to a *Rosa*^{Flippase} line (Jax 007844) to excise the Neo cassette. Neo cassette-negative progeny (verified via PCR of genomic DNA) were mated to C57 or CD1 mice to establish the line.

506

507 **Genetic labeling of MrgprD^{+} nociceptors:**

508 To label MrgprD^{+} nociceptors, *MrgprD^{CreERT2}* mice carrying the relevant reporter
509 allele were treated with tamoxifen (Sigma, T5648) pre- or postnatally. For prenatal
510 treatment, pregnant females were given tamoxifen along with estradiol (Sigma,
511 E8875, at a 1:1000 mass estradiol: mass tamoxifen ratio) and progesterone (Sigma,
512 P3972, at a 1:2 mass progesterone: mass tamoxifen ratio) in sunflower seed oil via
513 oral gavage at E16.5-E17.5, when *MrgprD* is highly expressed in mouse
514 non-peptidergic nociceptors[57]. For postnatal treatment, 0.5mg tamoxifen extracted in
515 sunflower seed oil was given via i.p. injection once per day from P10-P17 (or
516 P14-P21 for spinal cord slice recording experiments, Figure 6). At least one week was
517 given to drive recombination and reporter gene expression.

518

519 **Tissue preparation and histology**:

520 Procedures were conducted as previously described[58]. Briefly, mice used for
521 immunostaining or AP staining were euthanized with CO_2 and transcardially perfused
522 with 4% PFA/PBS, and dissected tissue (either skin or spinal cord and DRGs) was
523 post-fixed for 2 hr in 4% PFA/PBS at 4° C. Tissue used for immunostaining was
524 cryo-protected in 30% sucrose/PBS (4% overnight) before freezing. Mice used for *in*
525 *situ* hybridization were euthanized and unfixed dissected tissue was frozen. Frozen
526 glabrous skin and DRG/spinal cord sections (20-30 μm) were cut on a Leica CM1950

cryostat. Immunostaining of sectioned DRG, spinal cord, and glabrous skin tissue, whole mount skin immunostaining, and double fluorescence *in situ* hybridization was performed as described previously[58, 59]. The following antibodies and dyes were used: chicken anti-GFP (Aves, GFP-1020), rabbit anti-GFP (Invitrogen, A-11122), rabbit anti-NF200 (Sigma, N4142), rabbit anti-CGRP (Immunostar, 24112), conjugated IB4-Alex488 (Molecular Probes, I21411), chicken anti-peripherin (Aves, PER), chicken anti-PAP (Aves, PAP), mouse anti-PKCγ (Novex, 13-3800), rabbit anti-RET (IBL, 18121), rabbit anti-RFP (Chemicon, AB3216). *MrgprD*, *MrgprA3*, and *MrgprB4 in situ* probes were previously described[60].

Tissue (skin or spinal cord with attached DRGs) for whole mount AP colorimetric staining with BCIP/NBT substrate (Roche, 1138221001 and 11383213001) and for fluorescent staining with HNPP/FastRed substrate (Roche, 11758888001) was treated as previously described[59]. Following AP colorimetric labeling, tissue was either cleared in BABB for imaging or sectioned using a VT1200S vibratome (Leica Microsystems, Nussloch, Germany) (200 μm), followed by BABB clearing for imaging. Fluorescent labeled DRGs co-stained using antibodies were cleared in glycerol and for imaging.

Electrophysiology

Spinal cord slices recordings were conducted as previously described [61]. Basically, 4-6pw *MrgprD*^{CreERT2}; *Rosa*$^{ChR2\text{-}EYFP/ChR2\text{-}EYFP}$ or *MrgprD*^{CreERT2} ; *Rosa*$^{ChR2\text{-}EYFP/+}$ mice were anesthetized with a ketamine/xylazine/acepromazine cocktail. Laminectomy was performed, and the spinal cord lumbar segments were removed and placed in ice-cold incubation solution consisting of (in mM) 95 NaCl, 1.8 KCl, 1.2 KH_2PO_4, 0.5 $CaCl_2$, 7 $MgSO_4$, 26 $NaHCO_3$, 15 glucose, and 50 sucrose, oxygenated with 95% O_2 and 5% CO_2, at a pH of 7.35–7.45 and an osmolality of 310–320 mosM. Sagittal or transverse spinal cord slices (300-500 μm thick) were prepared using a VT1200S vibratome (Leica Microsystems, Nussloch, Germany) and incubated in 34°C incubation solution for 30 min.

The slice was transferred to the recording chamber and continuously perfused with recording solution at a rate of 3–4 ml/min. The recording solution consisted of (in mM) 127 NaCl, 1.8 KCl, 1.2 KH_2PO_4, 2.4 $CaCl_2$, 1.3 $MgSO_4$, 26 $NaHCO_3$, and 15 glucose, oxygenated with 95% O_2 and 5% CO_2, at a pH of 7.35–7.45 and an osmolality of 300–310 mosM. Recordings were performed at RT. Spinal cord slices were visualized with an Olympus BX 61WI microscope (Olympus Optical, Tokyo, Japan), and the substantia gelatinosa (lamina II), which is a translucent band across the dorsal horn, was used as a landmark. Fluorescently labeled ChR2-EYFP terminals in the DH were identified by epifluorescence, and neurons in this innervation territory were recorded in the whole cell patch-clamp configuration. Glass pipettes (3–5 MΩ) were filled with

internal solution consisting of (in mM) 120 K-gluconate, 10 KCl, 2 MgATP, 0.5 NaGTP, 20 HEPES, 0.5 EGTA, and 10 phosphocreatine di(tris) salt at a pH of 7.29 and an osmolality of 300 mosM. All data were acquired using an EPC-9 patch-clamp amplifier and Pulse software (HEKA, Freiburg, Germany). Liquid junction potentials were not corrected. The series resistance was between 10 and 25 MΩ.

Light induced EPSCs ($EPSC_L$s) were elicited at a frequency of 2/min by 473nm laser illumination (10 mW, 0.1-5ms, Blue Sky Research, Milpitas, USA). Blue light was delivered through a 40X water-immersion microscope objective. Mono- or polysynaptic $EPSC_L$s were differentiated by 0.2 Hz light stimulation. We classified a connection as monosynaptic if the EPSC jitter (average standard deviation of the light-induced EPSCs latency from stimulation) < 1.6 ms[62, 63].

Optogenetic stimulation of MrgprD$^+$ nociceptors in paw and leg skin

To induce light-evoked behavior in freely moving animals, we used P10-P17 tamoxifen treated *MrgprD^{CreERT2}; Rosa$^{ChR2\text{-}EYFP/ChR2\text{-}EYFP}$* mice and control littermates (*Rosa$^{ChR2\text{-}EYFP/ChR2\text{-}EYFP}$*) who were also tamoxifen treated, but lacked the Cre-driver. All tested animals were between 2-6 months old. An additional control was to shine 532nm green laser light (Shanghai Laser and Optics Century, GL532T8-1000FC/ADR-800A) to the paw skin of both experimental groups. To induce light-evoked aversive behavior in MrgprD$^+$ neurites in the paw skin, 1 or 5mW

of 473nm blue light laser (Shanghai Laser and Optics Century, BL473T8-150FC/ADR-800A) was shined directly to the paw skin through a mesh bottom floor, with a cutoff time of 10 seconds. We tested different light waveforms and found that 10Hz sine waveform pulsing gave the best behavior responses. Thus, we used this waveform for all our behavior tests.

To induce light-evoked aversive behavior in MrgprD^{+} neurites in the leg skin, first, all hair was removed from the leg with Nair hair remover under light 3% isoflourane anesthesia, and animals were given two days before being tested again. For leg stimulation, 1, 5, 10, or 20mW of 473nm blue light laser, with 10Hz sine waveform pulsing, was shined directly to the leg skin. The cutoff time for this behavior assay is 10 seconds. For habituation to either paw or leg skin light stimulation, on the first two days, animals were habituated to the testing paradigm by being placed in the plexiglass testing chamber (11.5×11.5×16 cm) for 30 minutes each day. On the third testing day, animals were placed in the plexiglass testing chamber for 15 minutes prior to light stimulation. Green and blue light testing were performed on different days, but two weeks separated the paw and leg skin light stimulation. For all stimulation, the laser light was delivered via an FC/PC Optogenetic Patch Cable with a 200micrometer core opening (ThorLabs) and there was approximately 1cm of space between the cable terminal and the targeted skin area. Light power intensity for each experiment was measured with a Digital Power Meter with a 9.5mm aperture

611 (ThorLabs). For leg skin stimulation, power intensity was only slightly impeded by
612 the thin wall (0.02cm) of the plexiglass holding chamber, as measured by the Digital
613 Power Meter (Figure 7D).
614
615 To gain precise spatial and temporal resolution of behavior responses, we recorded
616 behaving animals at 500 frames/second with a high-speed camera (FASTCAM UX100
617 800K-M-4GB - Monochrome 800K with 4GB memory) and attached lens (Nikon
618 Zoom Wide Angle Telephoto 24-85mm f2.8). With a tripod with geared head for
619 Photron UX100, the camera was placed at a ~45degree angle at ~1-2 feet away from
620 the plexiglass holding chambers where mice performed behaviors. The camera was
621 maximally activated with far-red shifted 10mW LED light that did not disturb animal
622 behavior. All data were collected and annotated on a Dell laptop computer with
623 Fastcam NI DAQ software that is designed to synchronize Photron slow motion
624 cameras with the M series integrated BNC Data Acquisition (DAQ) units from
625 National Instruments.
626
627 **Image acquisition and data analysis:**
628 Images were acquired either on a Leica DM5000B microscope (bright field with a
629 Leica DFC 295 camera and fluorescent with a Leica 345 FX camera), on a Lecia
630 SP5II confocal microscope (fluorescent), or on a Leica M205 C stereoscope with a
631 Leica DFC 450 C camera (bright field). Image manipulation and figure generation

were performed in ImageJ, Adobe Photoshop and Adobe Illustrator. Cell number counting, nociceptor arbor measurements, and fluorescence measurements were performed in ImageJ. For section histology experiments, n = 3-6 sections per animal from 3 animals. Central arbor height/width measurements were taken to be the relevant axes of fitted ellipses. Column graphs, pie charts and scatter plots were generated in GraphPad Prism5. Column graphs show mean ± SEM. Statistical significance was analyzed using Student's *t*-tests, one-way ANOVA with Tukey's multiple comparisons or Chi-square tests in GraphPad Prism5. For DRG fluorescence intensity measurements, the average fluorescence of outlined cells was normalized to background fluorescence (Figure S6).

Acknowledgements:

We thank Peter Dong for illustrating the model in Figure 7. We also thank Greg Bashaw for reading and providing suggestions for this manuscript. This work was supported by National Institutes of Health (NIH) grant (NS083702, NS094224) and the Klingenstein-Simons Fellowship Award in the Neurosciences to W.L. and by NIH grant (NS092297) to W.O. I.A.S. was supported by NIH grant (K12GM081259) and Burroughs Wellcome Fund grant PDEP.

Author Contributions:

652 W.O., I.A.S., L.C., M.M. and W.L. contributed to experimental design and

653 interpretation. W.O. performed most of the histological experiments in this paper.

654 L.C. performed the spinal cord slice recording experiments. I.A.S. and J.B. performed

655 the optogenetic behavior assays. W.O., I.A.S., L.C., M.M. and W.L. wrote and

656 revised this manuscript.

657

658

659 **References:**

660 1. Johansson, R.S. & Vallbo, A.B. Tactile sensibility in the human hand: relative
661 and absolute densities of four types of mechanoreceptive units in glabrous skin. *J*
662 *Physiol* **286**, 283-300 (1979).
663 2. Johansson, R.S. & Vallbo, A.B. Spatial properties of the population of
664 mechanoreceptive units in the glabrous skin of the human hand. *Brain Res* **184**,
665 353-366 (1980).
666 3. Brown, P.B. & Koerber, H.R. Cat hindlimb tactile dermatomes determined with
667 single-unit recordings. *J Neurophysiol* **41**, 260-267 (1978).
668 4. Weinstein, S. Intensive and Extensive Aspects of Tactile Sensitivity as a Function
669 of Body Part, Sex and Laterality. in *The Skin Senses* (ed. D.R. Kenshalo) 195-218
670 (Charles C. Thomas Publishing, Springfield, IL, 1968).
671 5. Brown, P.B., Koerber, H.R. & Millecchia, R. From innervation density to tactile
672 acuity: 1. Spatial representation. *Brain Res* **1011**, 14-32 (2004).
673 6. Pare, M., Smith, A.M. & Rice, F.L. Distribution and terminal arborizations of
674 cutaneous mechanoreceptors in the glabrous finger pads of the monkey. *J Comp*
675 *Neurol* **445**, 347-359 (2002).
676 7. Rice, F.L., Kinnman, E., Aldskogius, H., Johansson, O. & Arvidsson, J. The
677 innervation of the mystacial pad of the rat as revealed by PGP 9.5
678 immunofluorescence. *J Comp Neurol* **337**, 366-385 (1993).
679 8. Mancini, F., Haggard, P., Iannetti, G.D., Longo, M.R. & Sereno, M.I.
680 Fine-grained nociceptive maps in primary somatosensory cortex. *J Neurosci* **32**,
681 17155-17162 (2012).
682 9. Mancini, F., *et al.* A fovea for pain at the fingertips. *Curr Biol* **23**, 496-500
683 (2013).
684 10. Mancini, F., *et al.* Whole-body mapping of spatial acuity for pain and touch. *Ann*
685 *Neurol* **75**, 917-924 (2014).
686 11. Schmidt, R., Schmelz, M., Ringkamp, M., Handwerker, H.O. & Torebjork, H.E.
687 Innervation territories of mechanically activated C nociceptor units in human skin. *J*
688 *Neurophysiol* **78**, 2641-2648 (1997).
689 12. Schmidt, R., Schmelz, M., Weidner, C., Handwerker, H.O. & Torebjork, H.E.
690 Innervation territories of mechano-insensitive C nociceptors in human skin. *J*
691 *Neurophysiol* **88**, 1859-1866 (2002).
692 13. Bessou, P. & Perl, E.R. Response of cutaneous sensory units with unmyelinated
693 fibers to noxious stimuli. *J Neurophysiol* **32**, 1025-1043 (1969).
694 14. Beitel, R.E. & Dubner, R. Response of unmyelinated (C) polymodal nociceptors
695 to thermal stimuli applied to monkey's face. *J Neurophysiol* **39**, 1160-1175 (1976).
696 15. Treede, R.D., Meyer, R.A. & Campbell, J.N. Comparison of heat and mechanical
697 receptive fields of cutaneous C-fiber nociceptors in monkey. *J Neurophysiol* **64**,
698 1502-1513 (1990).

16. Lynn, B. & Carpenter, S.E. Primary afferent units from the hairy skin of the rat hind limb. *Brain Res* **238**, 29-43 (1982).
17. Lynn, B. & Shakhanbeh, J. Properties of A delta high threshold mechanoreceptors in the rat hairy and glabrous skin and their response to heat. *Neurosci Lett* **85**, 71-76 (1988).
18. Sugiura, Y., Lee, C.L. & Perl, E.R. Central projections of identified, unmyelinated (C) afferent fibers innervating mammalian skin. *Science* **234**, 358-361 (1986).
19. Sugiura, Y., Terui, N. & Hosoya, Y. Difference in distribution of central terminals between visceral and somatic unmyelinated (C) primary afferent fibers. *J Neurophysiol* **62**, 834-840 (1989).
20. Szentagothai, J. Neuronal and Synaptic Arrangement in the Substantia Gelatinosa Rolandi. *J Comp Neurol* **122**, 219-239 (1964).
21. Rethelyi, M. Preterminal and terminal axon arborizations in the substantia gelatinosa of cat's spinal cord. *J Comp Neurol* **172**, 511-521 (1977).
22. Cavanaugh, D.J., *et al.* Distinct subsets of unmyelinated primary sensory fibers mediate behavioral responses to noxious thermal and mechanical stimuli. *Proc Natl Acad Sci U S A* **106**, 9075-9080 (2009).
23. Liu, Q., *et al.* Mechanisms of itch evoked by beta-alanine. *J Neurosci* **32**, 14532-14537 (2012).
24. Zylka, M.J., Rice, F.L. & Anderson, D.J. Topographically distinct epidermal nociceptive circuits revealed by axonal tracers targeted to Mrgprd. *Neuron* **45**, 17-25 (2005).
25. Liu, Y., *et al.* Mechanisms of compartmentalized expression of Mrg class G-protein-coupled sensory receptors. *J Neurosci* **28**, 125-132 (2008).
26. Wright, D.E., Zhou, L., Kucera, J. & Snider, W.D. Introduction of a neurotrophin-3 transgene into muscle selectively rescues proprioceptive neurons in mice lacking endogenous neurotrophin-3. *Neuron* **19**, 503-517 (1997).
27. Molliver, D.C., *et al.* IB4-binding DRG neurons switch from NGF to GDNF dependence in early postnatal life. *Neuron* **19**, 849-861 (1997).
28. Zylka, M.J., *et al.* Prostatic acid phosphatase is an ectonucleotidase and suppresses pain by generating adenosine. *Neuron* **60**, 111-122 (2008).
29. Wu, H., Williams, J. & Nathans, J. Morphologic diversity of cutaneous sensory afferents revealed by genetically directed sparse labeling. *Elife* **1**, e00181 (2012).
30. Koerber, H.R. & Brown, P.B. Somatotopic organization of hindlimb cutaneous nerve projections to cat dorsal horn. *J Neurophysiol* **48**, 481-489 (1982).
31. Molander, C. & Grant, G. Cutaneous projections from the rat hindlimb foot to the substantia gelatinosa of the spinal cord studied by transganglionic transport of WGA-HRP conjugate. *J Comp Neurol* **237**, 476-484 (1985).
32. Cervero, F. & Connell, L.A. Distribution of somatic and visceral primary afferent fibres within the thoracic spinal cord of the cat. *J Comp Neurol* **230**, 88-98 (1984).

740 33. Brown, P.B. & Fuchs, J.L. Somatotopic representation of hindlimb skin in cat
741 dorsal horn. *J Neurophysiol* **38**, 1-9 (1975).
742 34. Brown, P.B., *et al.* Somatotopic organization of single primary afferent axon
743 projections to cat spinal cord dorsal horn. *J Neurosci* **11**, 298-309 (1991).
744 35. Swett, J.E. & Woolf, C.J. The somatotopic organization of primary afferent
745 terminals in the superficial laminae of the dorsal horn of the rat spinal cord. *J Comp*
746 *Neurol* **231**, 66-77 (1985).
747 36. Takahashi, Y., *et al.* Organization of cutaneous ventrodorsal and rostrocaudal
748 axial lines in the rat hindlimb and trunk in the dorsal horn of the spinal cord. *J Comp*
749 *Neurol* **445**, 133-144 (2002).
750 37. Takahashi, Y., Aoki, Y. & Doya, H. Segmental somatotopic organization of
751 cutaneous afferent fibers in the lumbar spinal cord dorsal horn in rats. *Anat Sci Int* **82**,
752 24-30 (2007).
753 38. Woolf, C.J. & Fitzgerald, M. Somatotopic organization of cutaneous afferent
754 terminals and dorsal horn neuronal receptive fields in the superficial and deep laminae
755 of the rat lumbar spinal cord. *J Comp Neurol* **251**, 517-531 (1986).
756 39. Grueber, W.B., Jan, L.Y. & Jan, Y.N. Tiling of the Drosophila epidermis by
757 multidendritic sensory neurons. *Development* **129**, 2867-2878 (2002).
758 40. Sagasti, A., Guido, M.R., Raible, D.W. & Schier, A.F. Repulsive interactions
759 shape the morphologies and functional arrangement of zebrafish peripheral sensory
760 arbors. *Curr Biol* **15**, 804-814 (2005).
761 41. Cui, L., *et al.* Identification of Early RET+ Deep Dorsal Spinal Cord Interneurons
762 in Gating Pain. *Neuron* **91**, 1137-1153 (2016).
763 42. Catania, K.C. & Kaas, J.H. Somatosensory fovea in the star-nosed mole:
764 behavioral use of the star in relation to innervation patterns and cortical
765 representation. *J Comp Neurol* **387**, 215-233 (1997).
766 43. Dong, X., Han, S., Zylka, M.J., Simon, M.I. & Anderson, D.J. A diverse family
767 of GPCRs expressed in specific subsets of nociceptive sensory neurons. *Cell* **106**,
768 619-632 (2001).
769 44. Han, L., *et al.* A subpopulation of nociceptors specifically linked to itch. *Nat*
770 *Neurosci* **16**, 174-182 (2013).
771 45. Liu, Q., *et al.* Sensory neuron-specific GPCR Mrgprs are itch receptors mediating
772 chloroquine-induced pruritus. *Cell* **139**, 1353-1365 (2009).
773 46. Liu, Q., *et al.* Molecular genetic visualization of a rare subset of unmyelinated
774 sensory neurons that may detect gentle touch. *Nat Neurosci* **10**, 946-948 (2007).
775 47. Zylka, M.J., Dong, X., Southwell, A.L. & Anderson, D.J. Atypical expansion in
776 mice of the sensory neuron-specific Mrg G protein-coupled receptor family. *Proc Natl*
777 *Acad Sci U S A* **100**, 10043-10048 (2003).
778 48. Badea, T.C., *et al.* Combinatorial expression of Brn3 transcription factors in
779 somatosensory neurons: genetic and morphologic analysis. *J Neurosci* **32**, 995-1007
780 (2012).

781 49. Li, L., *et al.* The functional organization of cutaneous low-threshold
782 mechanosensory neurons. *Cell* **147**, 1615-1627 (2011).
783 50. Scheibel, M.E. & Scheibel, A.B. Terminal axonal patterns in cat spinal cord. II.
784 The dorsal horn. *Brain Res* **9**, 32-58 (1968).
785 51. Shortland, P., Woolf, C.J. & Fitzgerald, M. Morphology and somatotopic
786 organization of the central terminals of hindlimb hair follicle afferents in the rat
787 lumbar spinal cord. *J Comp Neurol* **289**, 416-433 (1989).
788 52. Millecchia, R.J., *et al.* Influence of map scale on primary afferent terminal field
789 geometry in cat dorsal horn. *J Neurophysiol* **66**, 696-704 (1991).
790 53. Le Bars, D., Gozariu, M. & Cadden, S.W. Animal models of nociception.
791 *Pharmacol Rev* **53**, 597-652 (2001).
792 54. Badea, T.C., *et al.* New mouse lines for the analysis of neuronal morphology
793 using CreER(T)/loxP-directed sparse labeling. *PLoS One* **4**, e7859 (2009).
794 55. Madisen, L., *et al.* A robust and high-throughput Cre reporting and
795 characterization system for the whole mouse brain. *Nat Neurosci* **13**, 133-140 (2010).
796 56. Madisen, L., *et al.* A toolbox of Cre-dependent optogenetic transgenic mice for
797 light-induced activation and silencing. *Nat Neurosci* **15**, 793-802 (2012).
798 57. Chen, C.L., *et al.* Runx1 determines nociceptive sensory neuron phenotype and is
799 required for thermal and neuropathic pain. *Neuron* **49**, 365-377 (2006).
800 58. Fleming, M.S., *et al.* The majority of dorsal spinal cord gastrin releasing peptide
801 is synthesized locally whereas neuromedin B is highly expressed in pain- and
802 itch-sensing somatosensory neurons. *Mol Pain* **8**, 52 (2012).
803 59. Niu, J., *et al.* Modality-based organization of ascending somatosensory axons in
804 the direct dorsal column pathway. *J Neurosci* **33**, 17691-17709 (2013).
805 60. Luo, W., *et al.* A hierarchical NGF signaling cascade controls Ret-dependent and
806 Ret-independent events during development of nonpeptidergic DRG neurons. *Neuron*
807 **54**, 739-754 (2007).
808 61. Cui, L., *et al.* Modulation of synaptic transmission from primary afferents to
809 spinal substantia gelatinosa neurons by group III mGluRs in GAD65-EGFP transgenic
810 mice. *J Neurophysiol* **105**, 1102-1111 (2011).
811 62. Doyle, M.W. & Andresen, M.C. Reliability of monosynaptic sensory
812 transmission in brain stem neurons in vitro. *J Neurophysiol* **85**, 2213-2223 (2001).
813 63. Wang, H. & Zylka, M.J. Mrgprd-expressing polymodal nociceptive neurons
814 innervate most known classes of substantia gelatinosa neurons. *J Neurosci* **29**,
815 13202-13209 (2009).
816
817
818
819

820 **Figure Legends:**

821 **Figure 1.** *MrgprD*^{CreERT2} mice can mediate recombination specifically in adult

822 MrgprD^{+} non-peptidergic nociceptors. (A) Knock-in *MrgprD*^{CreERT2} allele. (B)

823 Illustration showing tamoxifen treatment scheme, 0.5 mg tamoxifen / day, P10-P17

824 treatment of *MrgprD*^{CreERT2}; *Rosa*$^{ChR2\text{-}EYFP}$ mice. (C) Triple staining of DRG section

825 showing EYFP overlaps with IB4 but not CGRP. (D-F) Double fluorescent *in situ*

826 DRG sections showing EYFP in *MrgprD* (D) but not *MrgprA3* (E) or *MrgprB4* (F)

827 cells. Pie charts show overlap quantification (% of EYFP^{+} cells that co-express Mrgpr,

828 n = 3 animals). (G) DH section showing EYFP^{+} terminal overlap with IB4 but not

829 CGRP. Arrowheads show overlapping cells, arrows show non-overlapping cells.

830 Scale bars = 50μm (C-F), 100μm (G).

831

832 **Figure 2.** Sparse MrgprD^{+} nociceptor labeling in untreated 3-4 pw *MrgprD*^{CreERT2};

833 *Rosa*^{iAP} mice. (A&B) Whole mount AP DRG staining of thoracic (A) and L5 (B)

834 DRGs. (C) AP^{+} cells / DRG for cervical (C), thoracic (T), and lumbar (L) DRGs, n =

835 47 DRGs from 3 animals. (D-H) Whole mount DRG immunostaining plus AP

836 fluorescent staining. Sparse AP^{+} cells express non-peptidergic nociceptor markers

837 peripherin (D), RET (F) and PAP (H) but not large diameter neuron maker NF200 (E)

838 or peptidergic marker CGRP (G). (I) Whole mount EGFPf immunostaining plus AP

839 fluorescence staining of untreated *MrgprD*$^{CreERT2/EGFPf}$; *Rosa*^{iAP} DRGs. AP^{+} neurons

840 are MrgprD^{+} nociceptors. Quantification of overlap (% of AP^{+} cells that co-express

841 *MrgprD*^{EGFPf}, n = 126 neurons from 3 animals). Scale bars = 50μm.

Figure 3. Peripheral organization of non-peptidergic nociceptors in 3-4 pw *MrgprD*^{CreERT2}; *Rosa*^{iAP} mice. **(**A, B, D, E) Sparse labeled non-peptidergic nociceptors show bushy-ending structure in the glabrous skin (A-B) and trunk hairy skin (D-E). B, E, high magnification images of regions boxed in A and D, respectively. (C, F) High-density labeled (0.5mg tamoxifen at P11) glabrous and hairy skin. Overall neurite densities are lower in glabrous compared to hairy skin. Red arrowheads in E&F mark neurite clumps that likely surround hair follicles. (G) Arbor areas in different skin regions. n = 173 terminals from 9 animals. * = p<0.05 (one-way ANOVA with Tukey's multiple comparisons test). (H) Arbor areas in the hind limb skin vs. proximodistal distance (D_{elbow}) from the elbow (point 0, terminals distal to this edge are given negative D_{elbow} values). n = 52 arbors from 4 animals. No clear relationship between proximodistal location and size is evident. Scale bars = 100μm.

Figure 4. Sparsely labeled *MrgprD*^{CreERT2}; *Rosa*^{iAP} nociceptors have region-specific central arbor morphologies. **(**A-F) Round and long non-peptidergic central arbors seen in top-down whole mount (A, C, D, F) and transverse section (B&E) spinal cords. Round arbors are in the medial lumbar enlargement (B&C) while long arbors are in the lateral lumbar enlargement and thoracic spinal cord (B-F). Dorsal roots are outlined and labeled in C. Red dashed lines outline the round arbor zone. Orange arrowhead marks a round terminal, purple arrowheads mark long terminals. M, medial. L, lateral. R, rostral. C, caudal. (G) Round and long (defined by ratio in H) arbor areas

are comparable for all regions. (H) Arbor Width/Height ratios by ganglion of origin. Round terminals: W/H > 0.2. *n* =368 terminals from 7 animals (I) Comparison of the number of labeled arbors in the hindlimb digit and plantar paw skin with the number of ipsilateral round terminals in the dorsal horn. *n* = 4 animals, dotted line shows 1:1 relationship. (J) Illustration showing the distribution of round (orange zone) and long (purple zone) arbors in the spinal cord. Scale bars = 50µm (A&B, D&E), 250µm (C&F).

Figure 5. Non-peptidergic nociceptor labeling with increasing densities reveals somatotopic organization of MrgprD^{+} central arbors. (A-F) AP staining of *MrgprD*^{CreERT2}; *Rosa*^{iAP} thoracic (A-C) and lumbar (D-F) spinal cords that received prenatal 0mg (A&D), 0.25mg (B&E) or 0.5mg (C&F) prenatal tamoxifen. Even with increased labeling densities, round and long arbors occupy exclusive zones of the DH. *n* = 3 animals per treatment. Scale bars = 250µm.

Figure 6. Plantar paw circuits show a heightened signal transmission in the dorsal horn. (A) Illustration of spinal cord slice recording from *MrgprD*^{CreERT2}; *Rosa*$^{ChR2\text{-}EYFP}$ mice (P14-P21 tamoxifen) using optical stimulation. Neuron cell bodies located in the territory innervated by EYFP^{+} fibers were chosen for recording. (B&C) Monosynaptic (B) and polysynaptic (C) light-induced EPSC ($EPSC_L$) traces recorded from layer II neurons during 0.2 Hz light stimulation (overlay of 20 traces). Light pulses indicated

by blue arrows, scale bars shown in lower right. (D) In *MrgprD*$^{CreERT2/+}$; *Rosa*$^{ChR2\text{-}EYFP/ChR2\text{-}EYFP}$ homozygous slices, similar incidences of light-responsive neurons were found in medial and lateral lumbar regions. (E) In *MrgprD*$^{CreERT2/+}$; *Rosa*$^{ChR2\text{-}EYFP/+}$ heterozygous slices, a much higher incidence of light-responsive neurons was seen in medial lumbar compared to lateral lumbar or medial thoracic circuits. (F) Frequency distribution of threshold light pulse durations required for eliciting $EPSC_L$s among cells in E. Among responsive cells, postsynaptic neurons in lateral lumbar and thoracic regions require longer pulse durations to be activated compared to those in medial lumbar region. Cell (*n*) numbers indicated in parentheses above bars in D-F.

Figure 7. Peripheral optogenetic activation of MrgprD^{+} nociceptors reveals regional differences in optical threshold required to elicit withdrawal responses. (A-C) Optical stimulation in the paw. (A) Representative whole-mount immunostaining of plantar paw skin in *MrgprD*$^{CreERT2/+}$; *Rosa*$^{ChR2\text{-}EYFP/ChR2\text{-}EYFP}$ mice, *n*=3 mice. (B) Schematic of light placement on paw skin, see videos. (C) Histogram showing percentage of mice displaying aversive responses to 5mW green light and 1 or 5mW blue light to littermate control *(C)* and *MrgprD*$^{CreERT2/+}$; *Rosa*$^{ChR2\text{-}EYFP/ChR2\text{-}EYFP}$ *(M)*. *n* = 6-10 for each genotype with 1-2 trials per mouse. * = p <0.001 Chi-square test. (D-F) Optical stimulation in the leg. (D) Representative whole-mount immunostaining of upper leg skin in *MrgprD*$^{CreERT2/+}$; *Rosa*$^{ChR2\text{-}EYFP/ChR2\text{-}EYFP}$ mice, *n* = 3 mice. Dotted lines outline

906 skin in *MrgprD*$^{CreERT2/+}$; *Rosa*$^{ChR2\text{-}EYFP/ChR2\text{-}EYFP}$ mice, *n* = 3 mice. Dotted lines outline
907 hair follicles (E) Schematic of light placement on hair-shaven leg skin, see videos. (F)
908 Histogram showing percentage of mice displaying aversive responses to 5, 10, or
909 20mW blue light at the leg (see above panel C for genotype description and statistical
910 analyses). (G) A lower activation threshold is required for paw versus leg skin
911 nociceptors. (H) Temporal delay time (seconds) from light onset to the first aversive
912 behavior with 5, 10, or 20mW blue light in paw or leg of *MrgprD*$^{CreERT2/+}$;
913 *Rosa*$^{ChR2\text{-}EYFP/ChR2\text{-}EYFP}$ mice. Error bars represent SEM. (I) Model showing
914 somatotopic organization of mammalian nociceptive circuitry. Distinct central arbor
915 morphologies ("round versus long") of MrgprD^{+} non-peptidergic nociceptors are
916 observed in the medial versus lateral dorsal spinal cord, which correlates well with
917 regional peripheral sensitivity and cortical representation. Scale bars = 50μm.
918
919 **Supplemental Figures and Videos:**
920 **Supplementary Figure S1**. Generation of *MrgprD*^{CreERT2} knock-in mouse line. (A)
921 Illustration showing the knock-in targeting strategy. Grey bar, 3' UTR Southern blot
922 probe site. P1, P2, primers for PCR screening. (B) Southern blot of SpeI-digested ES
923 genomic DNA, using a probe against *MrgprD* 3' UTR (grey bar in A). 4.3 kb,
924 *MrgprD*^{CreERT2} knock-in allele. 3.8 kb, *MrgprD* wild-type allele. (C) PCR screen of
925 electroporated ES clones, using P1, P2 primers. The positive PCR product is about 2
926 kb.

927

928 **Supplementary Figure S2.** Prenatal tamoxifen treatment labels MrgprD^{+} along with
929 MrgprA3/B4^{+} non-peptidergic DRG neurons. (A-D) Representative DRG sections of
930 3pw *MrgprD*^{CreERT2}; *Rosa*^{tdTomato} mice (2.5-5 mg tamoxifen at E16.5) immunostained
931 with the indicated markers. tdT^{+} neurons are positive for non-peptidergic neuron
932 markers peripherin (92.5 ± 4.0%) (A) and IB4 (85.6 ± 1.2%) (C), but do not express
933 NF200 (1.2 ± 0.01%) (B) or CGRP (1.4 ± 0.00%) (D). (E) Representative
934 immunostained DH section showing tdT^{+} fibers innervating layer II, ventral to
935 CGRP^{+} fibers but dorsal to PKCγ interneurons. (F-H) Double fluorescent *in situ*
936 shows expression of *MrgprD* (75.2 ± 0.8%) (F), *MrgprA3* (15.0 ± 0.2%) (G) and
937 *MrgprB4* (8.6 ± 0.1%) (H) in *tdT* expressing neurons from prenatally treated
938 *MrgprD*^{CreERT2}; *Rosa*^{tdTomato} mice (5 mg tamoxifen at E17.5). (I) Model showing
939 *MrgprD*^{CreERT2} specificity based on time of tamoxifen dosage. *MrgprD*^{CreERT2}
940 recombination is consistent with expression of *MrgprD* across development.
941 Arrowheads indicate marker overlap with tdT, arrows indicate tdT^{+} cells that do not
942 express indicated marker. Scale bars, 50µm (A-D, F-H), 100µm (E).

943

944 **Supplementary Figure S3.** Rare free arbors are found in sparsely labeled
945 non-peptidergic nociceptors of *MrgprD*^{CreERT2} ; *Rosa*^{iAP} mice. (A) Percentage of bushy
946 or free ending type arbors by location. *n* = 132 hairy, 22 glabrous terminals from 4

947 animals. (B&C) Sparse labeled free terminal-type arbor in trunk hairy skin. C is a
948 high magnification view of the region boxed in B. Scale bars = 100μm.
949
950 **Supplementary Figure S4.** Central arbors of sparsely labeled non-peptidergic
951 neurons in *MrgprD*^{CreERT2}; *Rosa*^{iAP} mice. (A&B) Examples of bifurcating
952 non-peptidergic nociceptor central projections from 1pw (0.05 mg tamoxifen at
953 E16.5) (A) and 3pw (B) spinal cords. Bifurcated branches sometimes give rise to
954 independent terminals (arrows in A), join other branches to give rise to a common
955 terminal (arrows in B) or end without elaborating a terminal (arrowhead in B). (C)
956 Round terminals in the upper cervical spinal cord and medulla, many of which
957 descend from the TG non-peptidergic neurons. Scale bars, 50μm (A&B), 250μm (C).
958
959 **Supplemental Figure S5.** Neighboring non-peptidergic nociceptors overlap
960 extensively in the skin and spinal cord. **(**A-C) Whole mount immunostaining of
961 *MrgprD*$^{CreERT2/EGFPf}$; *Rosa*^{tdTomato} (0.5 mg tamoxifen at E16.5) hairy skin with
962 anti-GFP and anti-RFP antibodies. The terminal field of one non-peptidergic
963 nociceptor is labeled with tdT, as outlined in A. B&C show higher magnifications
964 view of the regions boxed in A (solid line = B, dotted line = C). Innervation of hair
965 follicles is shown in C. (D) Immunostaining of a section of glabrous skin. (E&F)
966 Immunostaining of medial cervical (D) and thoracic (E) spinal cord sections, showing

sparse labeled round terminal and long terminals. Scale bars = 100μm (A), 20μm (B-F).

Supplementary Figure S6. MrgprD^{+} neurons show no regional difference in *Rosa*$^{ChR2\text{-}EYFP}$ expression. (A&B). Native (no immunostaining) ChR2-EYFP fluorescence of *MrgprD*^{CreERT2}; *Rosa*$^{ChR2\text{-}EYFP}$ (P10-P17 tamoxifen) DRG sections. (C) T10-T12 and L4-L4 DRG cell body fluorescence frequency distributions overlap, indicating no regional change in ChR2-EYFP expression level. Scale bars = 100μm.

Supplementary Figure S7. *In vivo* optogenetic peripheral stimulation. (A-C) *MrgprD*^{CreERT2}; *Rosa*$^{ChR2\text{-}EYFP}$ sectioned upper leg hairy skin (B) shows a higher density of ChR2-EYFP^{+} neurites than plantar paw glabrous skin (A). (C) Quantification of neurites per 100μm. n = 3 animals. * = p <0.05, Chi-square test. (D) Measured light power at three locations (closest side, midpoint, farthest side) in the behavior chamber with 5 mW, 10 mW, and 20 mW blue laser intensity. (E) Response rate (% of mice) showing withdrawal responses to 5 mW blue light stimulation at paw or upper leg. n = 6-10 mice, 1-2 trials per mouse. Scale bars = 50 μm (A&B).

Supplementary Video 1. High speed video recording of green laser light (5 mW) plantar paw stimulation of Control (*ChR2*) mice. Green light does not induce an avoidance response.

Supplementary Video 2. High speed video recording of green laser light (5 mW) plantar paw stimulation of *MrgprD*; *ChR2* mice. Green light does not induce an avoidance response.

Supplementary Video 3. High speed video recording of blue laser light (5 mW) plantar paw stimulation of Control mice. Blue light does not induce an avoidance response in Control mice.

Supplementary Video 4. High speed video recording of blue laser light (5 mW) plantar paw stimulation of *MrgprD*; *ChR2* mice. 5 mW blue laser light triggers robust avoidance responses, including paw withdrawal and shaking, when applied to the paw of *MrgprD*; *ChR2* mice.

Supplementary Video 5. High speed video recording of blue laser light (5 mW) shaved upper leg stimulation of Control mice. No avoidance response is seen.

Supplementary Video 6. High speed video recording of blue laser light (5 mW) upper leg stimulation of *MrgprD*; *ChR2* mice. 5 mW blue laser light is insufficient to trigger avoidance responses when applied to the shaved upper leg of *MrgprD*; *ChR2* mice.

Supplementary Video 7. High speed video recording of blue laser light (20mW) upper leg stimulation of Control mice. No avoidance response is seen, indicating that 20 mW laser light stimulation is not by itself aversive.

Supplementary Video 8. High speed video recording of blue laser light (20mW) upper leg stimulation of *MrgprD*; *ChR2* mice. 20 mW laser light induces robust avoidance behavior, including limb withdrawal and licking, when applied to the shaved upper leg of *MrgprD*; *ChR2* mice.

Figure 1

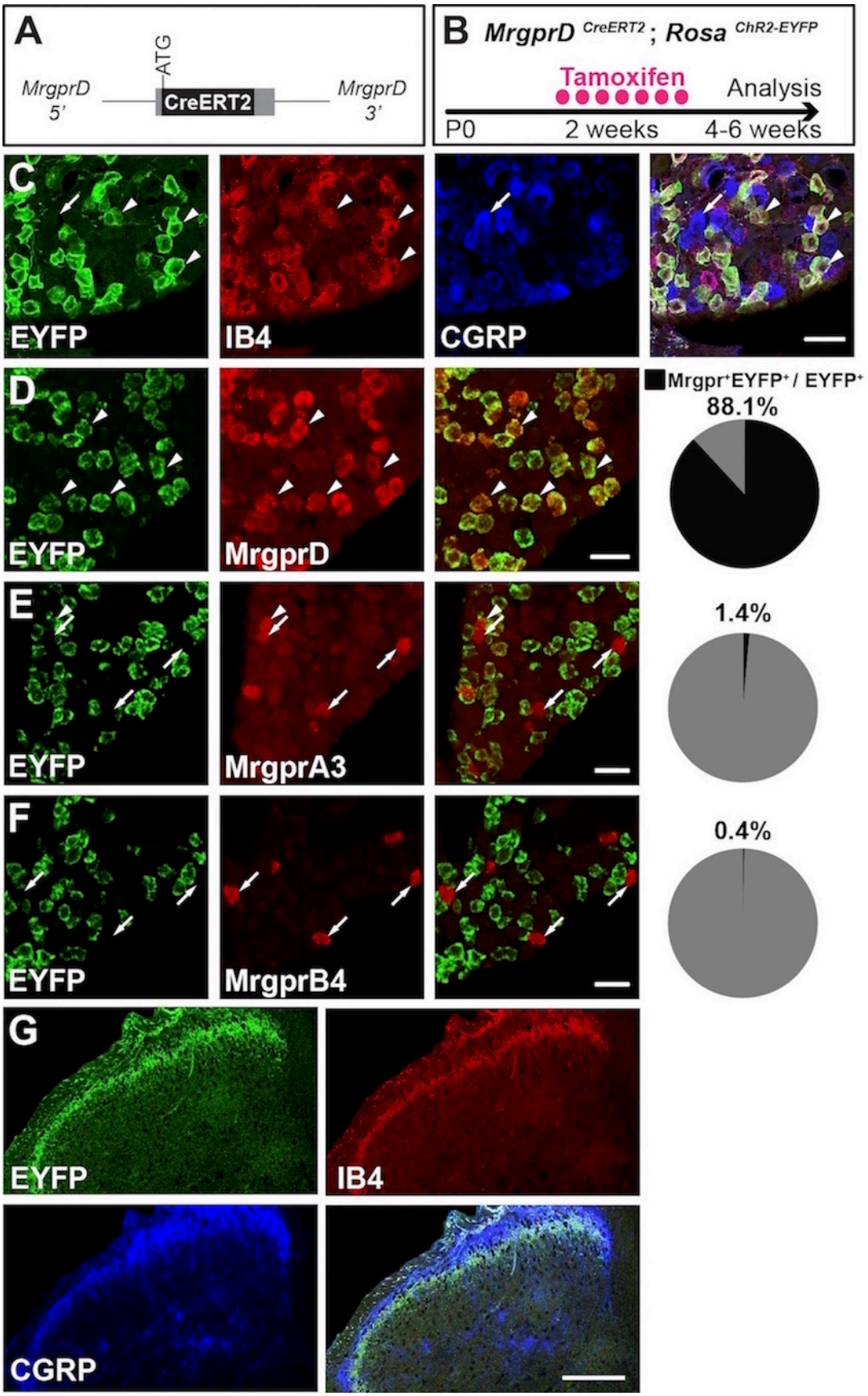
A
ATG
MrgprD 5'
CreERT2
MrgprD 3'
B MrgprD CreERT2 ; Rosa ChR2-EYFP
Tamoxifen
Analysis
P0
2 weeks
4-6 weeks
C
EYFP
IB4
CGRP
D
EYFP
MrgprD
Mrgpr+EYFP+ / EYFP+
88.1%
E
EYFP
MrgprA3
1.4%
F
EYFP
MrgprB4
0.4%
G
EYFP
IB4
CGRP

Figure 2

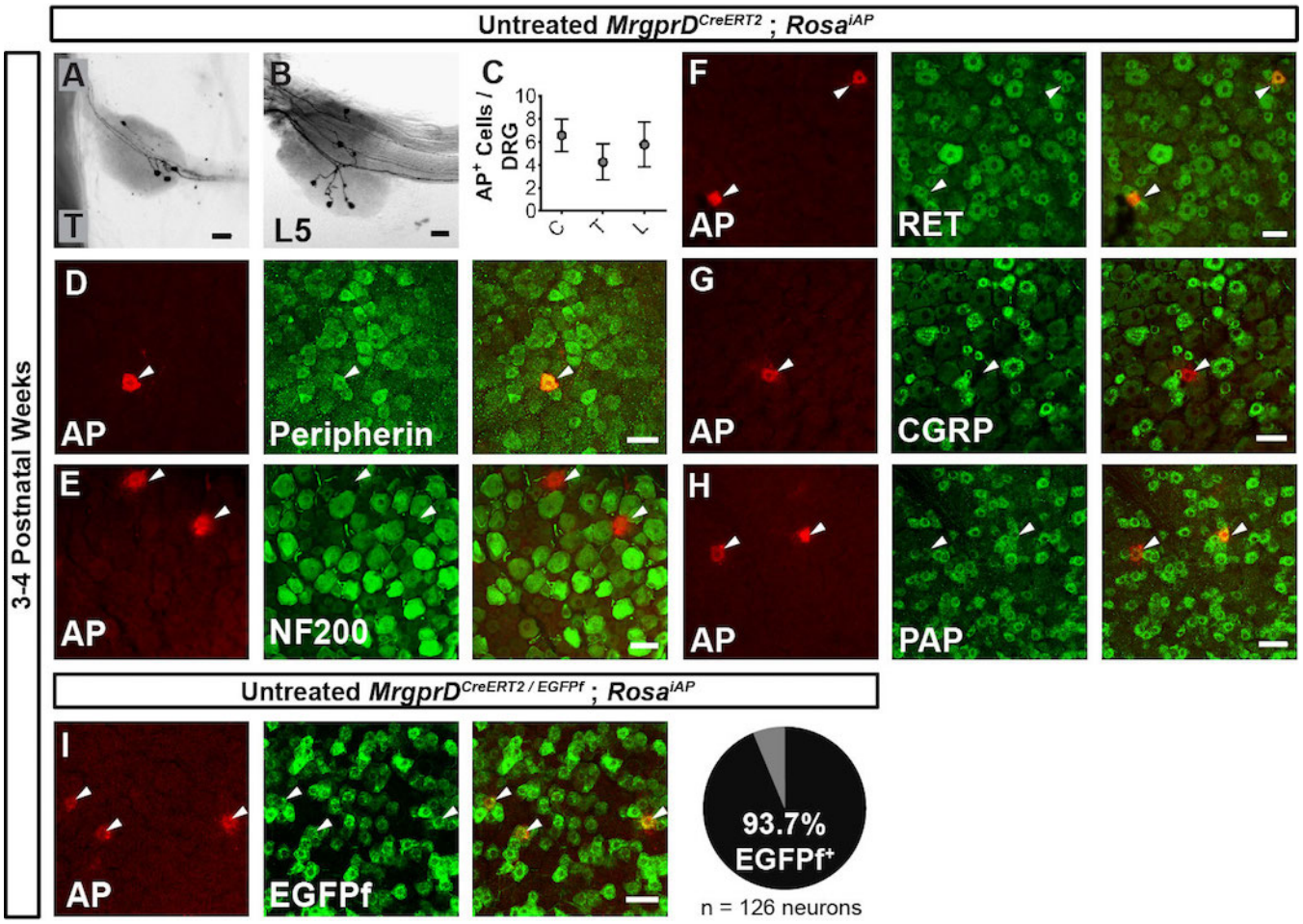
Untreated MrgprD^CreERT2 ; Rosa^iAP
3-4 Postnatal Weeks
A
T
B
L5
C
AP+ Cells / DRG
10
8
6
4
2
0
C
T
L
F
AP
RET
D
AP
Peripherin
G
AP
CGRP
E
AP
NF200
H
AP
PAP
Untreated MrgprD^CreERT2 / EGFPf ; Rosa^iAP
I
AP
EGFPf
93.7%
EGFPf+
n = 126 neurons

Figure 3

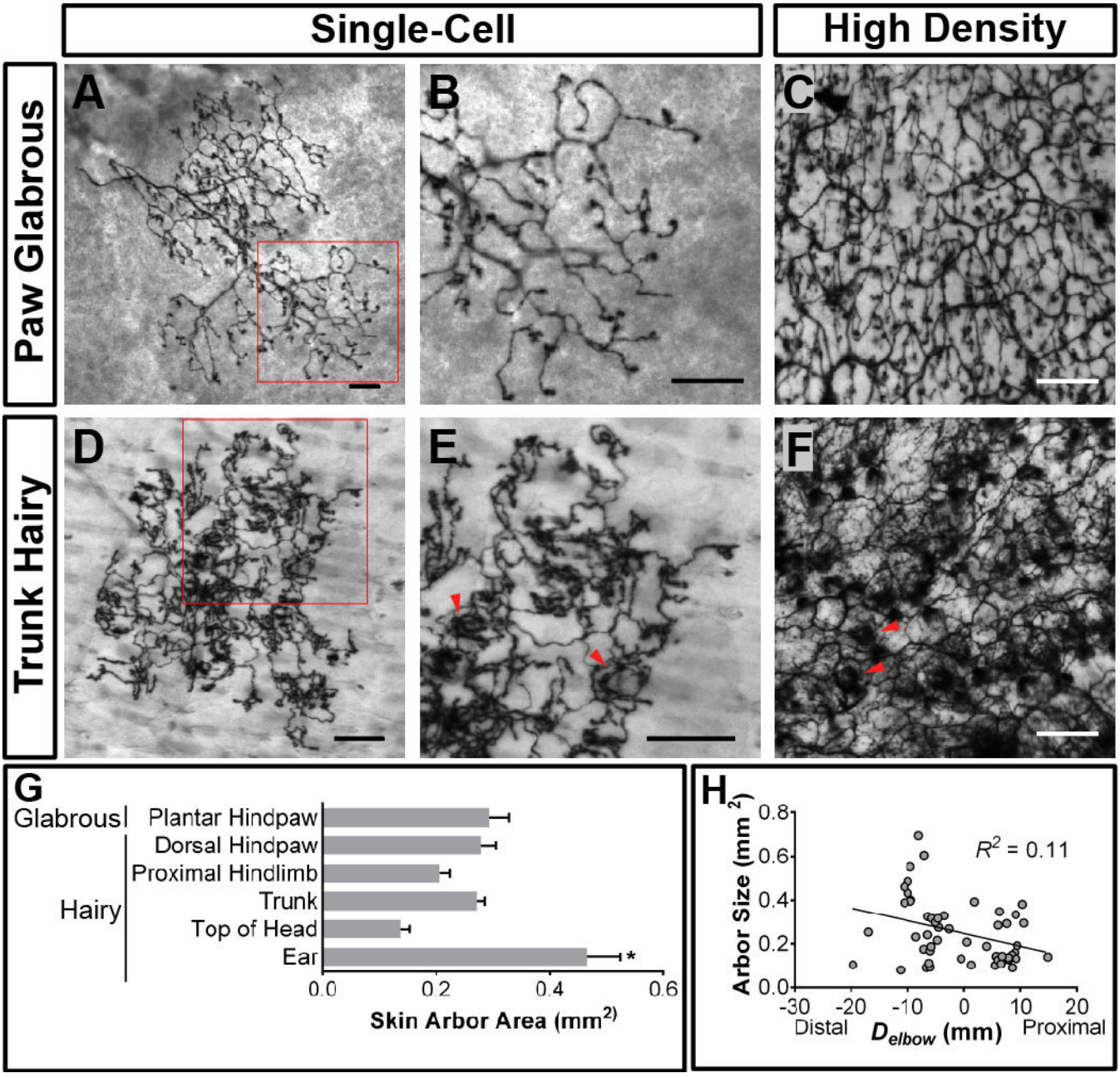
Single-Cell
High Density
Paw Glabrous
Trunk Hairy
A
B
C
D
E
F
G
Glabrous
Hairy
Plantar Hindpaw
Dorsal Hindpaw
Proximal Hindlimb
Trunk
Top of Head
Ear
*
0.0
0.2
0.4
0.6
Skin Arbor Area (mm2)
H
Arbor Size (mm2)
0.8
0.6
0.4
0.2
0.0
R2 = 0.11
-30
-20
-10
0
10
20
Distal
Delbow (mm)
Proximal

Figure 4

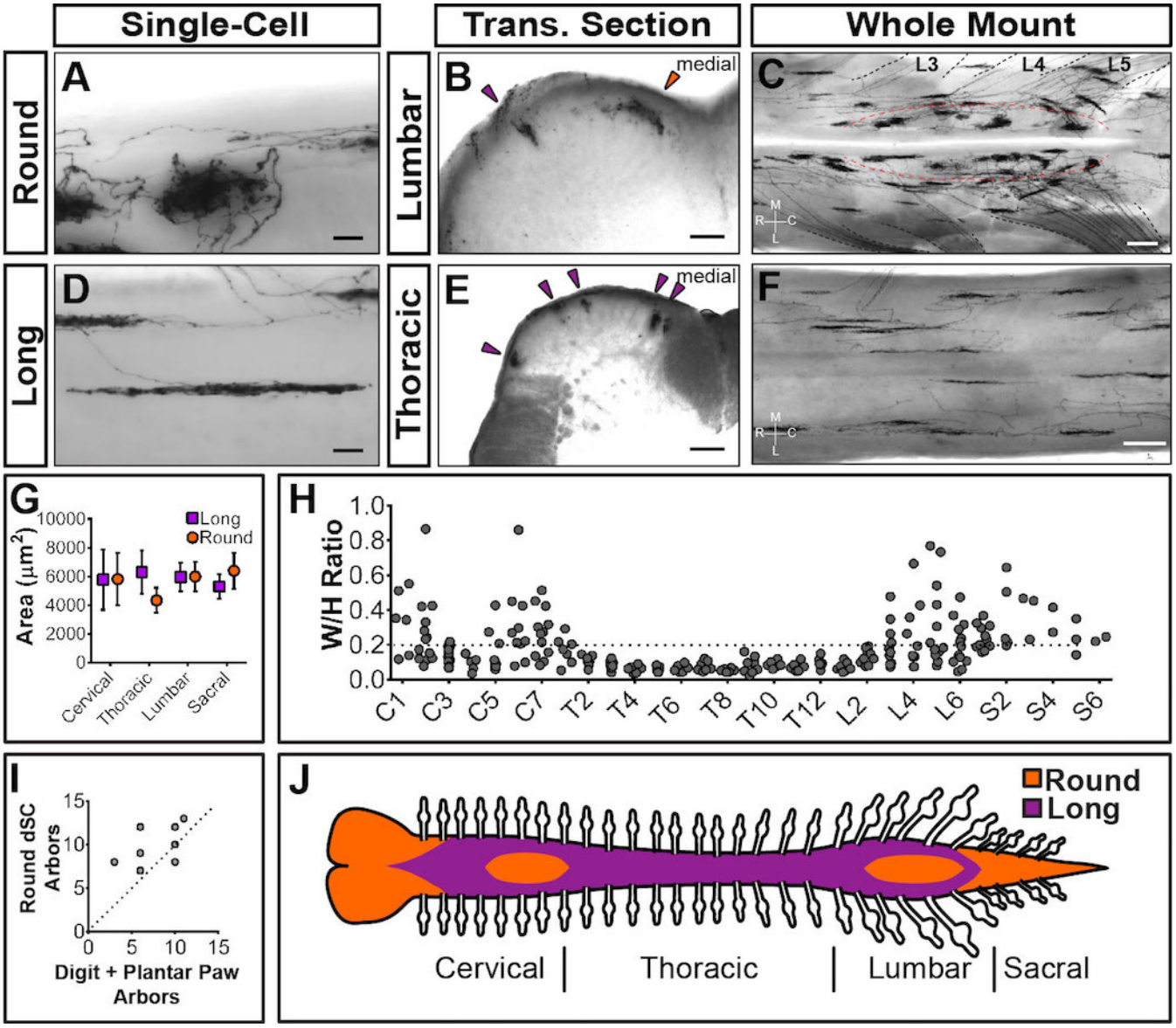
Single-Cell
Trans. Section
Whole Mount
Round
Lumbar
Long
Thoracic
A
B
C
D
E
F
medial
L3
L4
L5
G
Area (μm²)
Long
Round
Cervical
Thoracic
Lumbar
Sacral
H
W/H Ratio
C1
C3
C5
C7
T2
T4
T6
T8
T10
T12
L2
L4
L6
S2
S4
S6
I
Round dSC Arbors
Digit + Plantar Paw Arbors
J
Round
Long
Cervical
Thoracic
Lumbar
Sacral

Figure 5

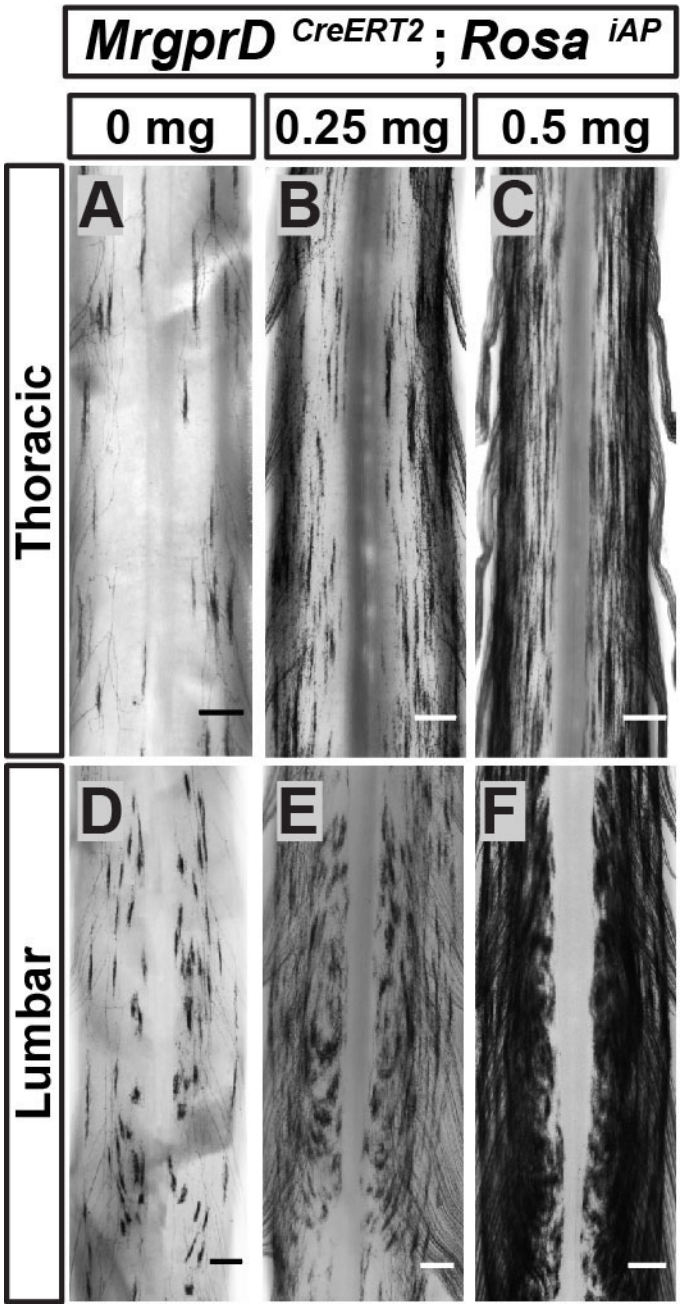
MrgprD CreERT2 ; Rosa iAP
0 mg
0.25 mg
0.5 mg
Thoracic
Lumbar
A
B
C
D
E
F

Figure 6

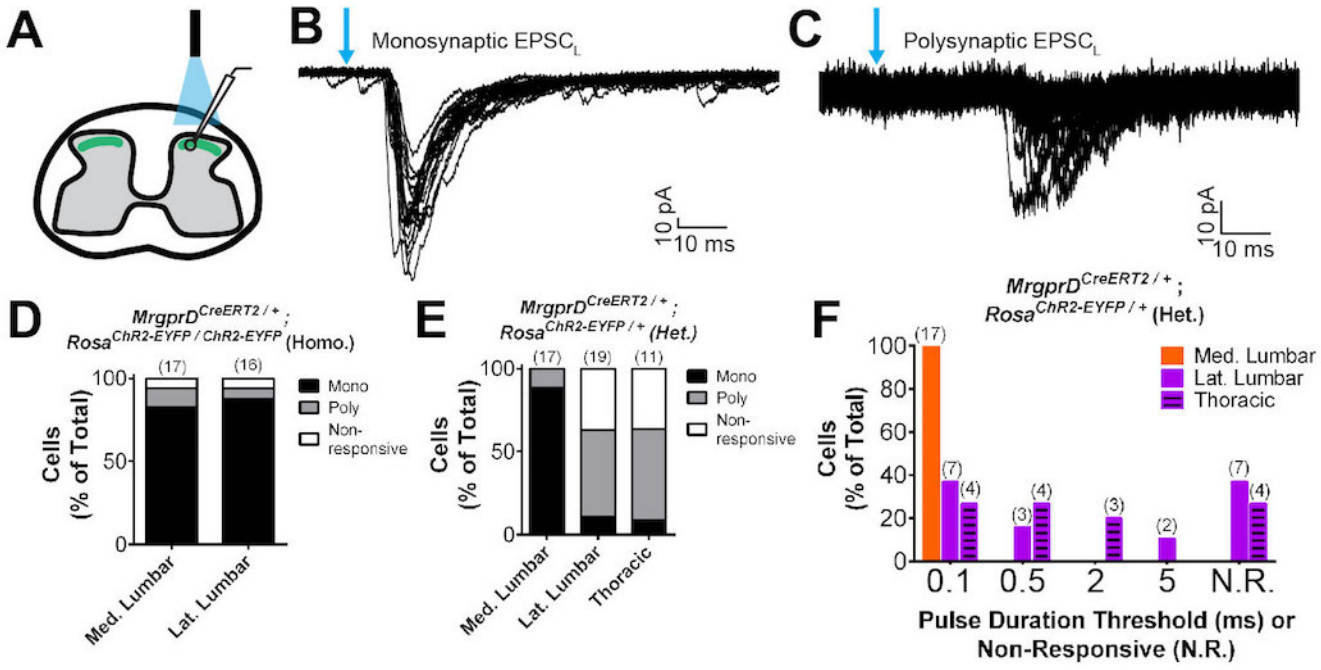
A
B
Monosynaptic EPSC$_L$
10 pA
10 ms
C
Polysynaptic EPSC$_L$
10 pA
10 ms
D
MrgprD$^{CreERT2/+}$; Rosa$^{ChR2\text{-}EYFP/ChR2\text{-}EYFP}$ (Homo.)
Cells (% of Total)
(17)
(16)
Mono
Poly
Non-responsive
Med. Lumbar
Lat. Lumbar
E
MrgprD$^{CreERT2/+}$; Rosa$^{ChR2\text{-}EYFP/+}$ (Het.)
(17)
(19)
(11)
Thoracic
F
MrgprD$^{CreERT2/+}$; Rosa$^{ChR2\text{-}EYFP/+}$ (Het.)
Med. Lumbar
Lat. Lumbar
Thoracic
0.1
0.5
2
5
N.R.
Pulse Duration Threshold (ms) or Non-Responsive (N.R.)

Figure 7

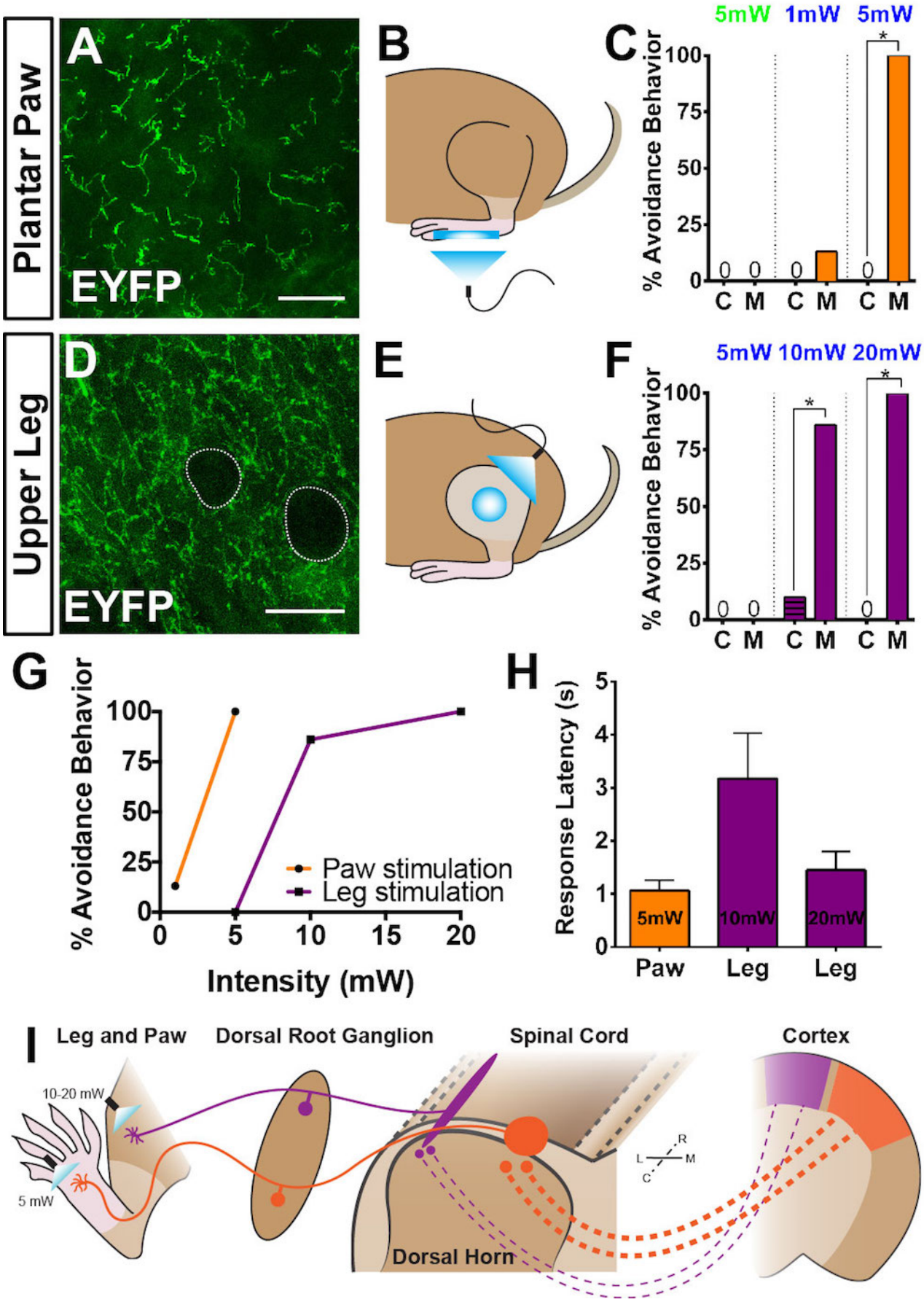
Plantar Paw
A
EYFP
B
C
5mW 1mW 5mW
% Avoidance Behavior
100
75
50
25
0
0 0 0 0
C M C M C M
*
Upper Leg
D
EYFP
E
F
5mW 10mW 20mW
% Avoidance Behavior
100
75
50
25
0
0 0
C M C M C M
*
*
G
% Avoidance Behavior
100
75
50
25
0
0 5 10 15 20
Intensity (mW)
Paw stimulation
Leg stimulation
H
Response Latency (s)
5
4
3
2
1
0
5mW
10mW
20mW
Paw Leg Leg
I
Leg and Paw
Dorsal Root Ganglion
Spinal Cord
Cortex
10-20 mW
5 mW
R
L
M
C
Dorsal Horn

Figure S1

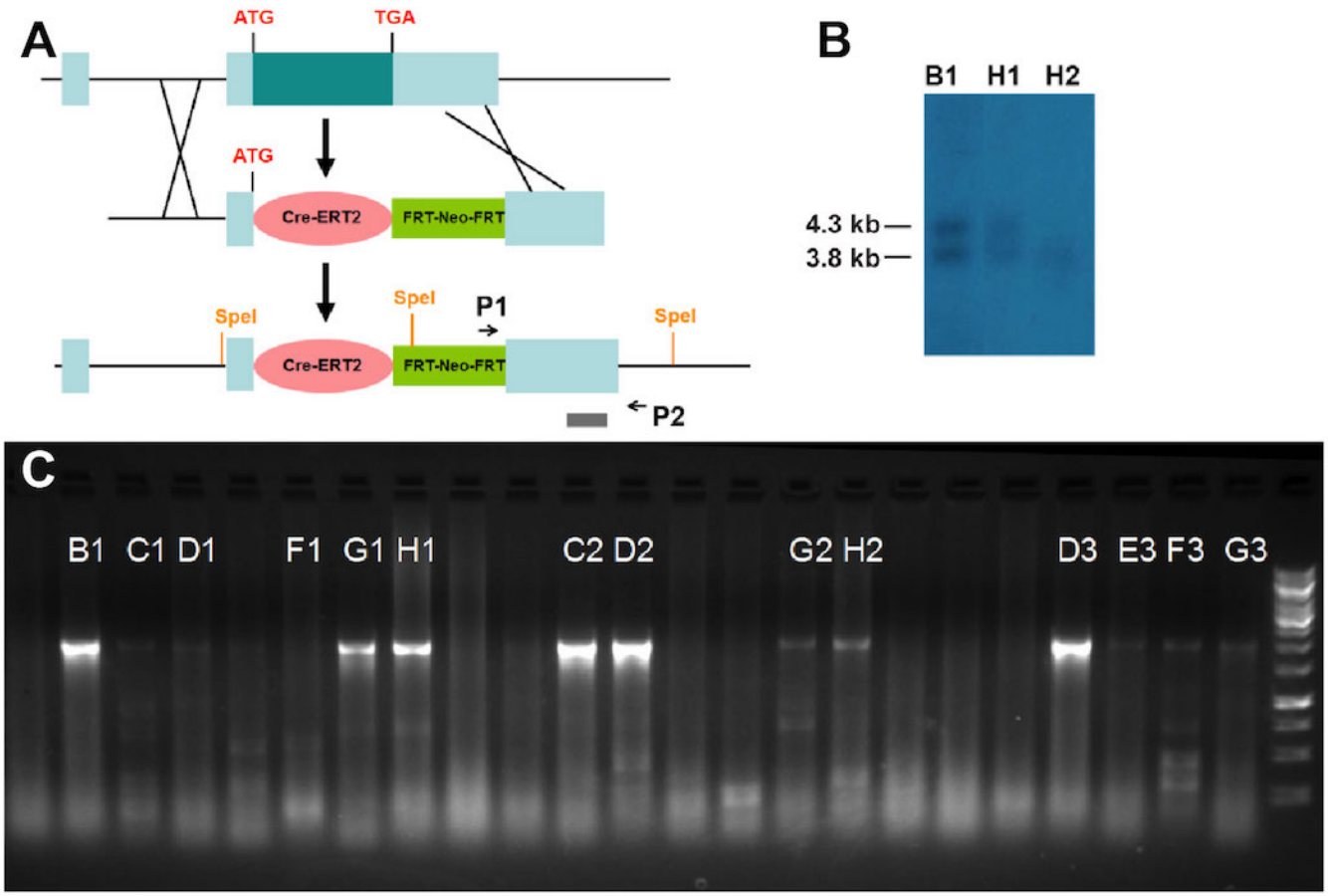
A
ATG
TGA
ATG
Cre-ERT2
FRT-Neo-FRT
SpeI
SpeI
P1
SpeI
Cre-ERT2
FRT-Neo-FRT
P2
B
B1 H1 H2
4.3 kb
3.8 kb
C
B1 C1 D1 F1 G1 H1 C2 D2 G2 H2 D3 E3 F3 G3

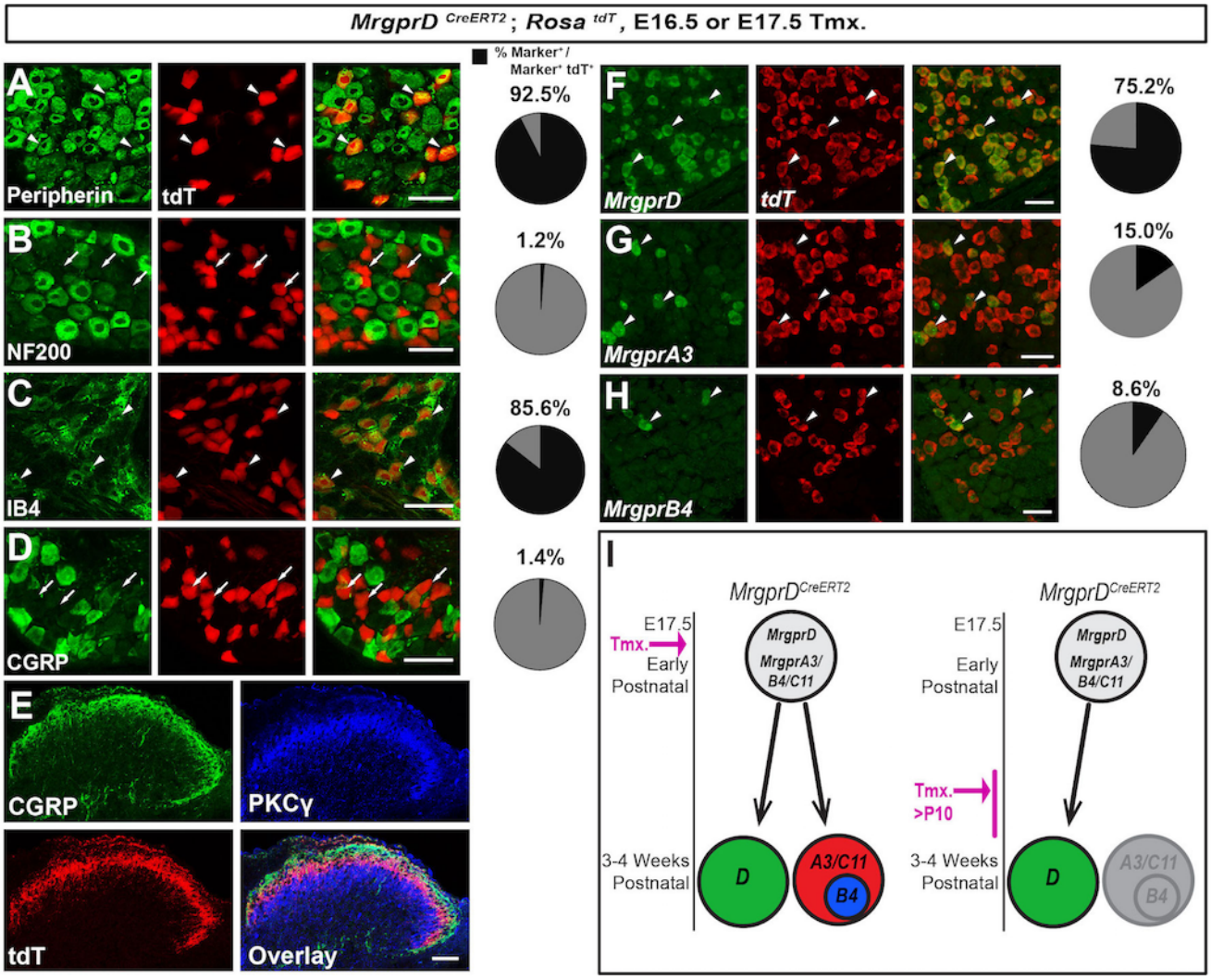
MrgprD CreERT2; Rosa tdT, E16.5 or E17.5 Tmx.
% Marker+ / Marker+ tdT+
A
Peripherin
tdT
92.5%
B
NF200
1.2%
C
IB4
85.6%
D
CGRP
1.4%
E
CGRP
PKCγ
tdT
Overlay
F
MrgprD
tdT
75.2%
G
MrgprA3
15.0%
H
MrgprB4
8.6%
I
MrgprDCreERT2
E17.5
Tmx.
Early Postnatal
MrgprD
MrgprA3/ B4/C11
3-4 Weeks Postnatal
D
A3/C11
B4
Tmx. >P10

Figure S2

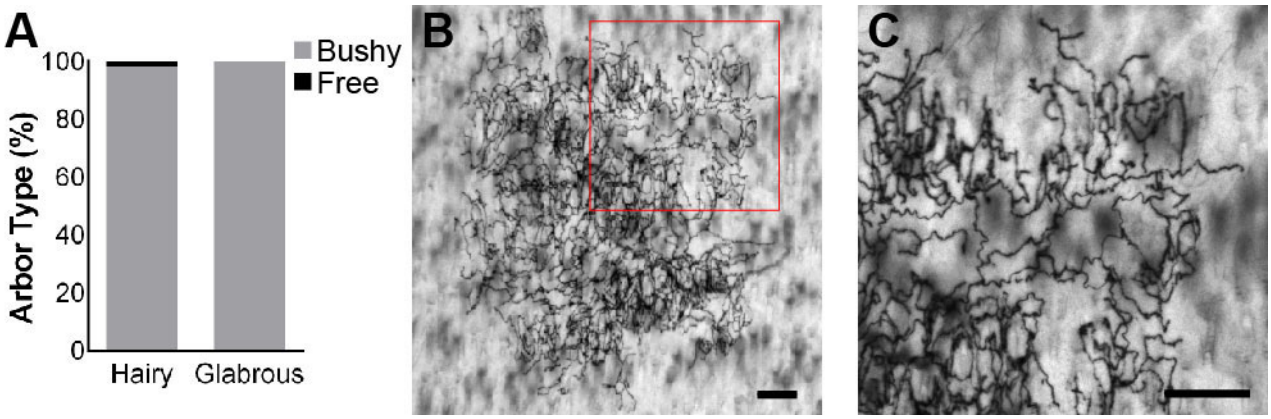

Figure S3

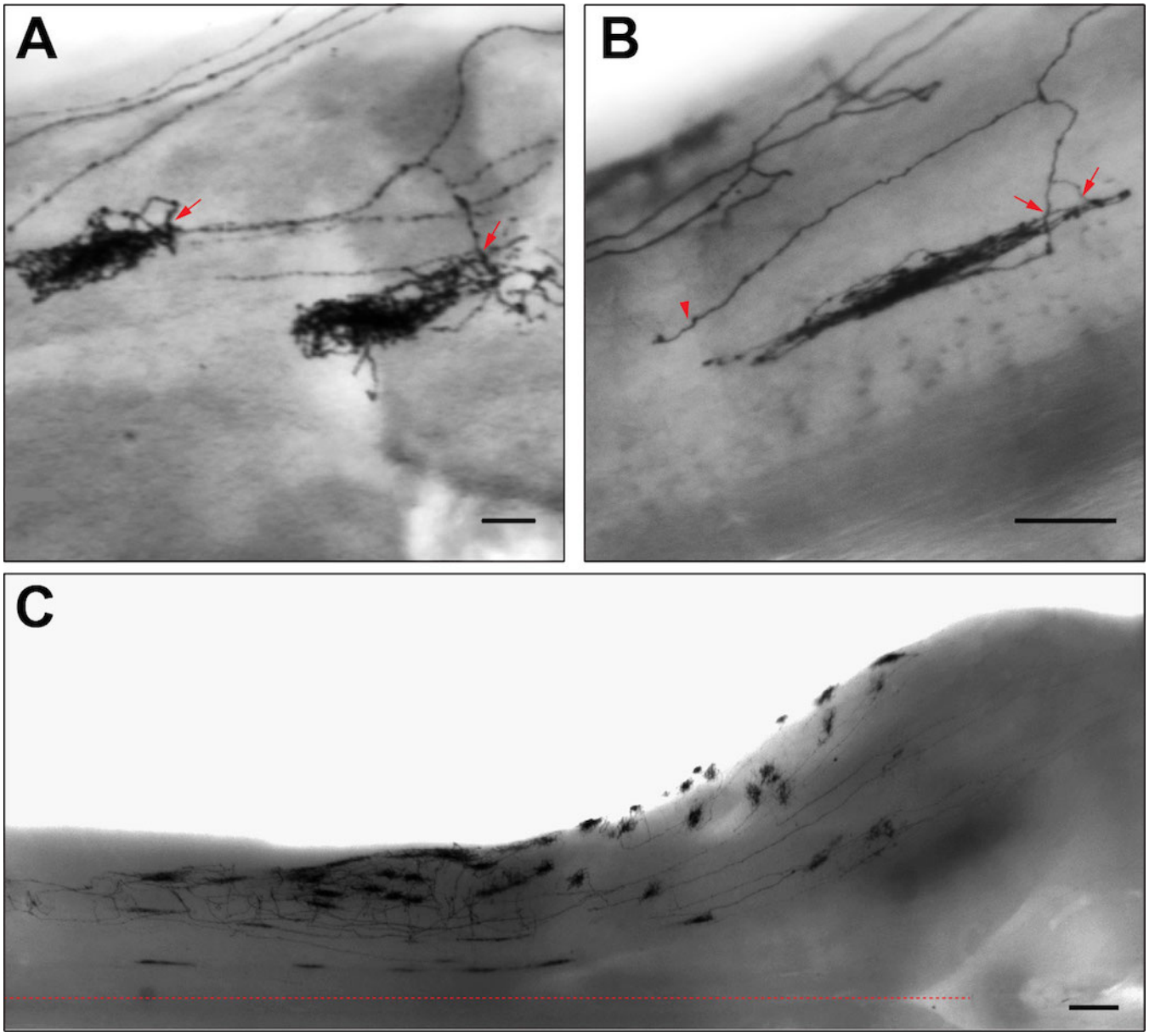

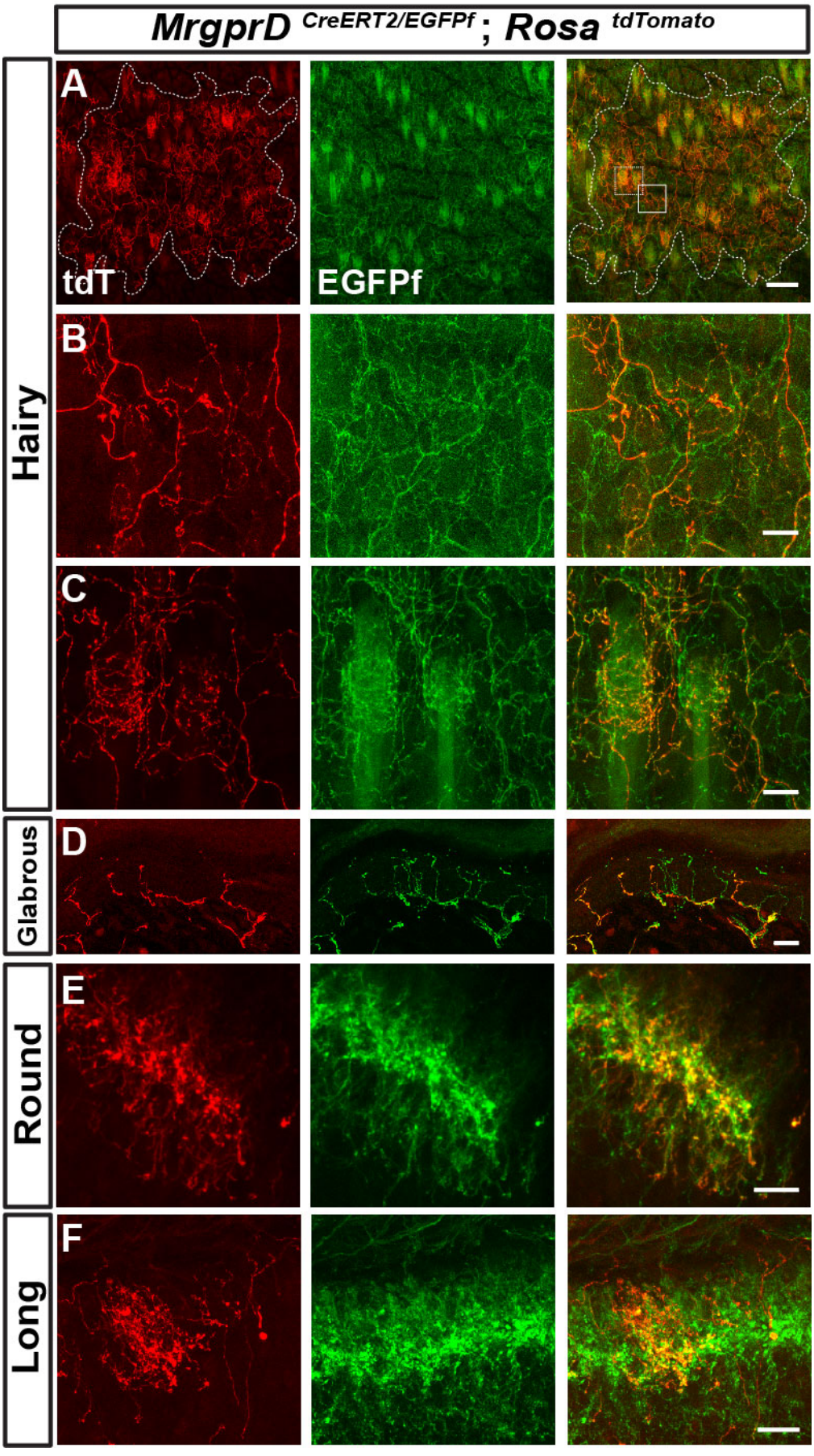
MrgprD CreERT2/EGFPf ; Rosa tdTomato
Hairy
Glabrous
Round
Long
A
B
C
D
E
F
tdT
EGFPf

Figure S5

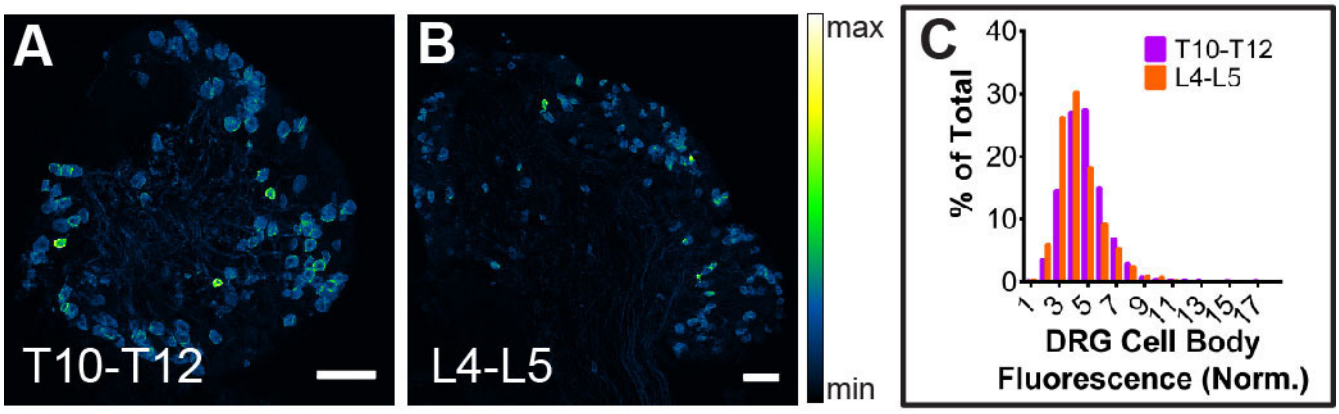
A
T10-T12
B
L4-L5
max
min
C
% of Total
40
30
20
10
0
T10-T12
L4-L5
1
3
5
7
9
11
13
15
17
DRG Cell Body
Fluorescence (Norm.)

Figure S6

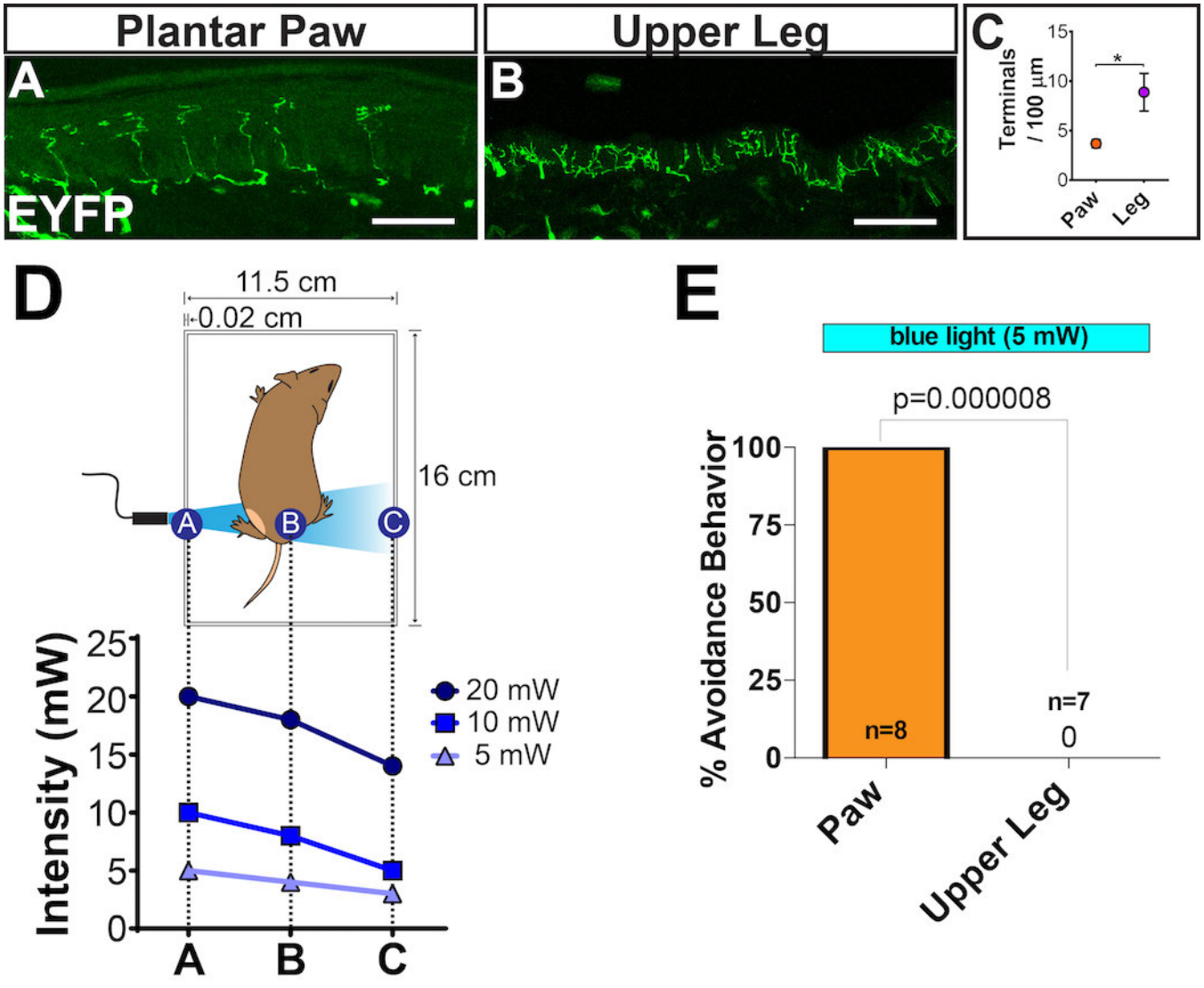
Plantar Paw
Upper Leg
A
B
EYFR
C
Terminals / 100 µm
15
10
5
0
*
Paw
Leg
D
11.5 cm
0.02 cm
16 cm
A
B
C
Intensity (mW)
25
20
15
10
5
0
20 mW
10 mW
5 mW
A
B
C
E
blue light (5 mW)
p=0.000008
% Avoidance Behavior
100
75
50
25
0
n=8
n=7
0
Paw
Upper Leg

Region	n	**Avg area (mm^2)**	SE	Min area (mm^2)	Max area (mm^2)
Plantar hindpaw (glabrous)	22	**0.29**	0.03	0.08	0.86
Dorsal hindpaw	27	**0.28**	0.03	0.15	0.54
Proximal hindlimb	29	**0.21**	0.02	0.14	0.32
Dorsal forepaw	9	**0.26**	0.07	0.11	0.45
Proximal forelimb	3	**0.14**	0.01	0.13	0.14
Trunk	77	**0.27**	0.01	0.10	0.9
Top of head	6	**0.14**	0.02	0.10	0.20
Ear*	11	**0.47**	0.06	0.22	0.93

Table 1. Summary of peripheral terminals of sparsely labeled MrgprD$^+$ non-peptidergic nociceptors. Data pooled from seven 3pw animals. Asterisk (*) indicates a significant difference (p<0.05, One-way ANOVA with Tukey's multiple comparison test) in average size in pair-wise comparisons with all other regions.

	n	% of Total
Total neurons	234	
Segments traveled from point of entry		
0	170	72.6
1	54	23.1
2	9	3.8
3	1	0.4
Direction traveled (for axons traveling 1-3 segments)		
Caudal	46	19.7
Rostral	18	7.7
No central branch bifurcations	154	65.8
1 central branch bifurcation	72	30.8
>1 central branch bifurcation	8	3.4
No central terminals	1	0.4
1 central terminals	215	91.9
2 central terminals	16	6.8
3 central terminals	2	0.9

Table 2. Summary of central innervation patterns of sparsely labeled MrgprD$^+$ non-peptidergic nociceptors. Data pooled from three 3pw animals.

	Round					Long				
	n	**Height (µm)**	SE	**Width (µm)**	SE	n	**Height (µm)**	SE	**Width (µm)**	SE
Cervical	31	**145**	28	**49**	11	45	**259**	56	**28**	5
Thoracic	3	**155**	6	**37**	6	81	**334**	61	**24**	4
Lumbar	99	**157**	20	**48**	5	83	**274**	32	**28**	3
Sacral	19	**162**	22	**51**	7	7	**197**	19	**35**	3

Table 3. Summary of non-peptidergic nociceptor central terminal height and width measurements. Round and long terminals were defined by W/H ratios (round = W/H ratio >0.2, long = W/H ratio <0.2). Data pooled from seven 3pw animals.

MrgprD^{CreERT2}; *Rosa*$^{ChR2\text{-}EYFP/ChR2\text{-}EYFP}$ (ChR2 Homozygous)

	Transverse			
	n	Mono $EPSC_L$	Poly $EPSC_L$	Non-Responsive
Medial Lumbar	15	11 (73.3%)	3 (20%)	1 (6.7%)
Lateral Lumbar	18	16 (88.9%)	1 (5.6%)	1 (5.6%)

MrgprD^{CreERT2}; *Rosa*$^{ChR2\text{-}EYFP/+}$ (ChR2 Heterozygous)

	Transverse			
	n	Mono $EPSC_L$	Poly $EPSC_L$	Non-responsive
Medial Lumbar	17	15 (88.2%)	2 (11.8%)	0 (0%)
Lateral Lumbar	19	2 (10.3%)	10 (52.6%)	7 (36.8%)
Thoracic	11	1 (9.1%)	6 (54.4%)	4 (36.4%)
	Sagittal			
	n	Mono $EPSC_L$	Poly $EPSC_L$	Non-responsive
Medial Lumbar	13	9 (69.2%)	3 (23.1%)	1 (7.7%)
Lateral Lumbar	16	0 (0%)	3 (18.8%)	13 (81.3%)
Thoracic	12	1 (8.3%)	3 (25.0%)	8 (66.7%)

Table 4. Summary of incidences of light-induced excitatory postsynaptic current ($EPSC_L$) responses recorded from layer II neurons in *MrgprD*^{CreERT2}; *Rosa*$^{ChR2\text{-}EYFP}$ homozygous and heterozygous mice. Patch clamp recordings were taken from either transverse or sagittal dSC slices, as indicated. Responses were classified as mono- or polysynaptic (see text). Shaded boxes show the response of the majority (>50%) of recorded cells.